

**DEVELOPMENT AND VALIDATION OF A COMPACT
BIODIESEL SURROGATE FUEL MODEL FOR MULTI-
DIMENSIONAL CFD APPLICATIONS**

POON HIEW MUN

**FACULTY OF ENGINEERING
UNIVERSITY OF MALAYA
KUALA LUMPUR**

2019

**DEVELOPMENT AND VALIDATION OF A COMPACT
BIODIESEL SURROGATE FUEL MODEL FOR MULTI-
DIMENSIONAL CFD APPLICATIONS**

POON HIEW MUN

**RESEARCH PROJECT SUBMITTED IN PARTIAL
FULFILMENT OF THE REQUIREMENTS FOR THE
DEGREE OF MASTER IN MECHANICAL
ENGINEERING**

**FACULTY OF ENGINEERING
UNIVERSITY OF MALAYA
KUALA LUMPUR**

2019

UNIVERSITY OF MALAYA
ORIGINAL LITERARY WORK DECLARATION

Name of Candidate : Poon Hiew Mun
Matric No : KQK170032
Name of Degree : Master in Mechanical Engineering
Title of Research Project : Development and Validation of a Compact Biodiesel
Surrogate Fuel Model for Multi-Dimensional CFD
Applications
Field of Study : Renewable Energy

I do solemnly and sincerely declare that:

- (1) I am the sole author/writer of this Work;
- (2) This Work is original;
- (3) Any use of any work in which copyright exists was done by way of fair dealing and for permitted purposes and any excerpt or extract from, or reference to or reproduction of any copyright work has been disclosed expressly and sufficiently and the title of the Work and its authorship have been acknowledged in this Work;
- (4) I do not have any actual knowledge nor do I ought reasonably to know that the making of this work constitutes an infringement of any copyright work;
- (5) I hereby assign all and every rights in the copyright to this Work to the University of Malaya ("UM"), who henceforth shall be owner of the copyright in this Work and that any reproduction or use in any form or by any means whatsoever is prohibited without the written consent of UM having been first had and obtained;
- (6) I am fully aware that if in the course of making this Work I have infringed any copyright whether intentionally or otherwise, I may be subject to legal action or any other action as may be determined by UM.

Candidate's Signature

Date:

Subscribed and solemnly declared before,

Witness's Signature

Date:

Name :

Designation :

DEVELOPMENT AND VALIDATION OF A COMPACT BIODIESEL SURROGATE FUEL MODEL FOR MULTI-DIMENSIONAL CFD APPLICATIONS

ABSTRACT

This work reports the development of a reduced biodiesel surrogate fuel model for multi-dimensional computational fluid dynamics (CFD) simulations. The model is derived using an integrated chemical kinetic mechanism reduction scheme and the final chemistry comprises 84 species with 264 elementary reactions. The model is first validated in zero-dimensional (0-D) chemical kinetic calculations under a wide range of auto-ignition and jet-stirred reactor (JSR) conditions. The ignition delays (ID) and species profiles computed by the reduced model are in well agreement with those of the detailed model. Apart from that, the experimental species profiles of rapeseed methyl ester (RME) oxidation in a JSR are also reasonably reproduced. Subsequently, the fidelity of the model is further assessed in two-dimensional (2-D) CFD simulations of a constant volume combustion chamber at two ambient temperatures of 900 K and 1000 K. The surrogate model is validated against the experimental results of soy-methyl ester (SME) combustion using the corresponding fuel compositions. Comparisons of the computations with the experimental measurements reveal that ID, lift-off lengths (LOL) and soot volume fractions are reasonably well replicated by the model. Following that, the applicability of the reduced model to serve as a universal surrogate model for other biodiesel feed-stocks, such as palm-methyl ester (PME) and sunflower-methyl ester (SFME), is investigated. The compositions of the reduced model are varied according to the saturation/unsaturation levels in each fuel. Each configuration is first validated in 0-D kinetic simulations, followed by the 2-D spray combustion simulations. The findings show that the calculated IDs and LOLs decrease with increasing unsaturation level. Soot

formation is also enhanced with the presence of greater amount of unsaturated ester. In this work, it is demonstrated that the reduced model can potentially be used to predict the reactivity of biodiesel feed-stocks with low degree of saturation ($\leq 30\%$) in both kinetic and CFD spray simulations.

Keywords: Chemical kinetics, mechanism reduction, biodiesel, spray combustion

University of Malaya

DEVELOPMENT AND VALIDATION OF A COMPACT BIODIESEL SURROGATE FUEL MODEL FOR MULTI-DIMENSIONAL CFD APPLICATIONS

ABSTRAK

Kerja ini melaporkan perkembangan model kinetik kimia yang ringkas untuk biodiesel bagi simulasi dinamik bendalir (CFD). Model ini dibina dengan menggunakan skim pengurangan mekanisme kinetik kimia bersepadu. Model terakhir terdiri daripada 84 spesis dengan 264 reaksi asas. Pertama, model ini disahkan dengan pengiraan kinetik kimia sifar-dimensi (0-D) di bawah pelbagai jenis reaktor auto-ignition dan reaktor jet-stirred (JSR). Ignition delay (ID) dan profil spesis yang dikira oleh model yang dibina adalah dalam persetujuan dengan model terperinci. Selepas itu, model ini diuji dengan lebih lanjut dalam simulasi dinamik bendalir dua-dimensi (2-D) dalam ruang pembakaran isipadu malar pada suhu 900 K dan 1000 K. Keputusan daripada simulasi telah dibandingkan dengan data eksperimen pembakaran soya metil ester (SME). ID, lift-off length (LOL) dan soot volume fraction (SVF) yang dikira oleh model adalah dalam persetujuan dengan data eksperimen. Selepas itu, kegunaan model ini sebagai model global bagi jenis metil ester yang lain seperti palm metil ester (PME) dan sunflower metil ester (SFME) telah disiasatkan. Komposisi model telah diubahkan mengikut tahap ketepuan bagi setiap jenis metil ester. Setiap konfigurasi telah disahkan dalam simulasi kinetik 0-D terlebih dahulu, diikuti dengan simulasi 2-D. Keputusan menunjukkan bahawa ID dan LOL yang dikira semakin kurang apabila tahap ketepuan ester semakin rendah. Pembentukan jelaga juga dipertingkatkan dengan tahap ketepuan ester yang lebih rendah. Dalam projek ini, keputusan yang diperolehi telah menunjukkan bahawa model yang dibina berpotensi digunakan untuk meramalkan kereaktifan biodiesel dengan tahap ketepuan yang rendah ($\leq 30\%$) bagi simulasi dinamik bendalir.

Kata kunci: Kinetik kimia, pengurangan mekanisme, biodiesel, pembakaran semburan

University of Malaya

ACKNOWLEDGEMENTS

I would like to express my sincere thanks to my project supervisor, Dr. Chong Wen Tong, for his support throughout the course of this study. Besides, I would also like to thank my family and friends for their encouragement and moral support throughout my studies.

University of Malaya

TABLE OF CONTENTS

Abstract	iii
Abstrak	v
Acknowledgements	vii
Table of Contents	viii
List of Figures	xii
List of Tables.....	xiv
List of Symbols and Abbreviations.....	xv
List of Appendices	xix
CHAPTER 1: INTRODUCTION.....	1
1.1 Background.....	1
1.1.1 Biodiesel Fuel Kinetics	2
1.1.2 Kinetic Model Reduction	2
1.2 Problem Statements	3
1.3 Research Questions.....	3
1.4 Aim and Objectives	4
1.5 Scope and Limitations	4
1.6 Outlines of the Thesis	4
CHAPTER 2: LITERATURE REVIEW.....	6
2.1 Introduction.....	6
2.2 Overviews on Actual Biodiesel Fuels.....	6
2.3 Various Kinetic Models for Biodiesel Fuels	9
2.4 Kinetic Model Reduction.....	10
2.5 Chapter Conclusions.....	14

CHAPTER 3: RESEARCH METHODOLOGY	16
3.1 Introduction.....	16
3.2 Methodology.....	16
3.2.1 Detailed Model of the Biodiesel Fuel.....	18
3.2.2 Five-Stage Chemical Kinetic Mechanism Reduction Scheme.....	19
3.2.3 Closed Homogeneous Batch Reactor Model and JSR Model in 0-D Simulations.....	22
3.2.4 CFD Sub-Models in 2-D Simulations	23
3.2.4.1 Spray Breakup Model.....	23
3.2.4.2 Turbulence Model	23
3.2.4.3 Soot Model	24
3.3 Project Schedule	25
3.4 Chapter Conclusions.....	26
CHAPTER 4: BIODIESEL FUEL SURROGATE MODEL FORMULATION....	27
4.1 Introduction.....	27
4.2 Fuel Constituents	27
4.3 Operating Conditions.....	28
4.4 Developmental Procedures of the Reduced Model	28
4.4.1 DRGEP	29
4.4.2 Isomer Lumping	29
4.4.3 Reaction Path Analysis.....	30
4.4.4 DRG.....	30
4.4.5 Adjustment of Reaction Rate Constants.....	31
4.5 Chapter Conclusions.....	32

CHAPTER 5: MODEL VALIDATIONS IN 0-D CHEMICAL KINETIC SIMULATIONS	33
5.1 Introduction.....	33
5.2 Operating Conditions.....	33
5.3 Validations against detailed model under auto-ignition Conditions.....	34
5.4 Validations against detailed model under JSR Conditions.....	36
5.5 Validations against JSR Experimental Measurements	38
5.6 Chapter Conclusions.....	40
CHAPTER 6: MODEL VALIDATIONS IN 2-D SPRAY COMBUSTION SIMULATIONS	41
6.1 Introduction.....	41
6.2 Model Formulations.....	41
6.2.1 Experimental Setups.....	41
6.2.2 Numerical Model Configurations.....	44
6.3 Validation Results Under Non-Reacting Fuel Spray Conditions	47
6.4 Validation Results Under Reacting Fuel Spray Conditions	47
6.5 Chapter Conclusions.....	49
CHAPTER 7: VARIATION IN FUEL SATURATION LEVELS.....	50
7.1 Introduction.....	50
7.2 Surrogate Fuel Compositions	50
7.3 Model Validations in 0-D Kinetic Simulations	51
7.3.1 Validations against Detailed Model under Auto-Ignition and JSR Conditions	51
7.3.2 Validations against JSR Experimental Data.....	55
7.4 2-D CFD Spray Combustion Simulations	57

7.5 Chapter Conclusions.....	59
CHAPTER 8: CONCLUSIONS AND FUTURE WORK	60
8.1 Conclusions	60
8.2 Suggestions for Future Work.....	61
References	62
List of Publications and Papers Presented	72
Appendix A: Reduced biodiesel fuel kinetic model	73

University of Malaya

LIST OF FIGURES

Figure 2.1: Hydrocarbon structures of the FAMEs (Bax et al., 2010).....	7
Figure 3.1: Flow chart of the research project.	17
Figure 3.2: Five-stage integrated chemical kinetic mechanism reduction scheme (Poon, 2016).	20
Figure 4.1: Example of one of the key reaction paths during fuel oxidation process.....	30
Figure 5.1: Comparisons of the IDs computed by the reduced (solid lines) and detailed (symbols) models under auto-ignition conditions at initial pressures of (a) 40 bar, (b) 60 bar, (c) 80 bar, Φ of 0.5 (green), 1 (black), 2 (red), over a temperature range of 650 K – 1350 K.	34
Figure 5.2: Comparisons of the computed species profiles by the reduced (solid lines) and detailed (symbols) models under auto-ignition conditions at initial pressure of 60 bar, Φ of 1, and temperature of 950 K.	35
Figure 5.3: Comparisons of the computed species mole fractions by the reduced (solid lines) and detailed (symbols) models under JSR conditions at pressure of 60 bar, Φ of 1, and t_R of 0.1 s over a temperature range of 650 K – 1350 K.	37
Figure 5.4: Comparisons of the computed and experimental species mole fractions of (a) CO, CO ₂ , and (b) CH ₄ , C ₂ H ₄ , C ₃ H ₆ obtained from RME oxidation in a JSR.....	39
Figure 6.1: Photograph (top) and a schematic cross-section (bottom) of the constant-volume combustion vessel (Siebers, 1998).....	42
Figure 6.2: Schematic diagram of the optical setup (Nerva et al., 2012).....	44
Figure 6.3: Wedge-shaped computational grid for the 2-D spray combustion simulations.	45
Figure 6.4: Comparisons of the predicted (green) and measured (black) LPL and VPL.	47
Figure 6.5: Predicted SVF contours and experimental soot cloud images at quasi-steady state for fuel combustions at ambient temperatures of 900 K and 1000 K. Note: Red lines indicate the flame lift-off.	49
Figure 7.1: Computed ID of (a) SME, (b) SFME and (c) PME calculated by respective detailed and reduced models, with initial pressure of 60 bar and Φ of (i) 0.5, (ii) 1.0, (iii) 2.0.....	52

Figure 7.2: Computed species profiles of (a) SME, (b) SFME and (c) PME fuel oxidations under auto-ignition conditions ($P=60$ bar, $\Phi=1.0$, $T=950$ K)..... 53

Figure 7.3: Computed species profiles of (a) SME, (b) SFME and (c) PME fuel oxidations under JSR conditions ($P=60$ bar, $\Phi=1.0$, $t_R=0.1$ s)..... 54

Figure 7.4: Computed and experimental species mole fractions obtained from the oxidation of (a) SME, (b) SFME and (c) PME in a JSR, with initial pressure of 106 kPa, Φ of 1.0 and t_R of 1.5 s. Note: The horizontal dashed lines (- -) indicate the maximum species mole fraction predicted by the surrogate model among SME, SFME and PME. 56

Figure 7.5: Experimental and simulated (a) IDs and (b) LOLs for RME, SME, SFME and PME combustions at ambient temperatures of 900 K (black) and 1000 K (red)..... 58

Figure 7.6: Experimental and simulated soot contours at quasi-steady state for RME, SME, SFME and PME combustions at ambient temperatures of (a) 900 K and (b) 1000 K..... 59

University of Malaya

LIST OF TABLES

Table 2.1: Average FAME compositions of different biodiesel fuels (Mishra & Solanki, 2016).	6
Table 2.2: Percentage of saturated and unsaturated FAME in the actual biodiesel fuels by mass (Herbinet et al., 2008).	7
Table 3.1: Project timelines.....	25
Table 4.1: Operating conditions applied during mechanism reduction process.	28
Table 4.2: Examples of isomers in the detailed kinetic model.	29
Table 4.3: Comparison of the original and adjusted A-factor values of Arrhenius parameters.	31
Table 5.1: Operating conditions for model validations in 0-D simulations.....	33
Table 6.1: Fuel injector characteristics.	43
Table 6.2: Experimental operating conditions under reacting and non-reacting ambient conditions. (Nerva et al., 2012; Siebers, 1998).	43
Table 6.3: Boundary conditions applied in the wedge mesh generation.....	46
Table 6.4: CFD sub-models applied in the 2-D spray combustion simulations.....	46
Table 6.5: Comparisons between the predicted and measured IDs and LOLs at ambient temperatures of 900 K and 1000 K.	48
Table 7.1: Compositions of the actual biodiesel fuels and the kinetic model (by mass).50	

LIST OF SYMBOLS AND ABBREVIATIONS

0-D	:	Zero-Dimensional
2-D	:	Two-Dimensional
C ₂ H ₂	:	Acetylene
C ₂ H ₄	:	Ethylene
CFD	:	Computational Fluid Dynamics
CME	:	Coconut Methyl Ester
CN	:	Cetane Number
CO	:	Carbon Monoxide
CO ₂	:	Carbon Dioxide
CSP	:	Computational Singular Perturbation
DIC	:	Direct Interaction Coefficient
DRG	:	Directed Relation Graph
DRGASA	:	Directed Relation Graph aided Sensitivity Analysis
DRGEP	:	Directed Relation Graph with Error Propagation
DRGEP SA	:	Directed Relation Graph with Error Propagation and Sensitivity Analysis
ECN	:	Engine Combustion Network
FAME	:	Fatty Acid Methyl Esters
H	:	Hydrogen Atom
H ₂	:	Hydrogen Molecule
H ₂ O	:	Hydrogen Oxide
H ₂ O ₂	:	Hydrogen Peroxide
HCO	:	Formyl
HO ₂	:	Hydroperoxyl

ID	:	Ignition Delay
ILDMM	:	Intrinsic Low Dimensional Manifold
JSR	:	Jet Stirred Reactor
LII	:	Laser-Induced Incandescence
LLNL	:	Lawrence Livermore National Laboratory
LOL	:	Lift-Off Length
LPL	:	Liquid Penetration Length
MB	:	Methyl Butanoate
MB2D	:	Methyl(E)-2-Butenoate
MD	:	Methyl Decanoate
MD5D	:	Methyl-5-Decenoate
MD9D	:	Methyl-9-Decenoate
N ₂	:	Nitrogen
NTC	:	Negative Temperature Coefficient
O ₂	:	Oxygen
OH	:	Hydroxyl
PAH	:	Polycyclic Aromatic Hydrocarbon
PCA	:	Principle Component Analysis
PME	:	Palm Methyl Ester
PSR	:	Perfectly-Stirred Reactor
RME	:	Rapeseed Methyl Ester
RNG	:	Re-Normalization Group
s	:	Second
SFME	:	Sunflower Methyl Ester
SME	:	Soy Methyl Ester
SVF	:	Soot Volume Fraction

VPL	:	Vapor Penetration Length
A	:	Pre-Exponential Factor [Vary depending on the order of reaction]
$C_{1\varepsilon}$:	Model Constants in Standard k - ε Model [-]
$C_{2\varepsilon}$:	Model Constants in Standard k - ε Model [-]
$C_{3\varepsilon}$:	Model Constants in Standard k - ε Model [-]
C_x	:	Overall Consumption Rate of Species x [mol/m ³ -s]
C_μ	:	Model Constants in Standard/RNG k - ε Model [-]
dM/dt	:	Net Soot Production Rate [kg/m ³ -s]
dN/dt	:	Instantaneous Production Rate of Soot Particles [particles/m ³ -s]
E_a	:	Activation Energy [J/mol]
F	:	Mass Fraction [-]
J	:	Total Number of Reactions [-]
k	:	Turbulence Kinetic Energy [m ² /s ²]
P_x	:	Overall Production Rate of Species x [mol/m ³ -s]
Re	:	Reynolds Number [-]
r_{xy}	:	Normalised Contribution of Species y to the Production Rate of Species x [-]
R_{xy}	:	Overall Interaction Coefficient [-]
S_k	:	User-defined source term for k in Standard k - ε Model [-]
S_ε	:	User-defined source term for ε in Standard k - ε Model [-]
T	:	Temperature [K]
T	:	Time [Units vary]
ω	:	Reaction Rate [Units vary]
β	:	Temperature Exponent [-]
ε	:	Dissipation Rate [m ² /s ³]
μ_{eff}	:	Effective Viscosity [kg/m-s]

μ_t	:	Turbulent Viscosity [kg/m-s]
ρ_g	:	Gas Density [kg/m ³]
σ_k	:	Turbulent Prandtl Numbers for Turbulent Kinetic Energy [-]
σ_ε	:	Turbulent Prandtl Numbers for Dissipation [-]
Φ	:	Equivalence Ratio [-]

University of Malaya

LIST OF APPENDICES

Appendix A: Reduced Biodiesel Fuel Kinetic Model	73
--	----

University of Malaya

CHAPTER 1: INTRODUCTION

1.1 Background

Of late, studies on alternative energy resources have actively progressed to pursue a solution for greenhouse gas emissions and depleting oil reserves. Among all, biodiesel has received significant attention and popularity worldwide as a cleaner alternative fuel to conventional diesel fuel owing to its great potential in reducing pollutant emissions, such as carbon oxides, unburned hydrocarbons and particulates. On top of that, its application is also compatible with the current diesel infrastructure as it can be used in existing diesel engines without additional engine modifications (Lee & Baik, 2014). It is noted that biodiesel is a renewable energy source which can be produced locally from biological resources such as vegetable oils and animal fats through transesterification process using an alcohol. In comparison to the conventional diesel fuel, it contains higher amount of oxygen contents in the fuel. It is reported that the presence of additional oxygen atoms in biodiesels may facilitate the combustion process in a diesel engine and the successive oxidations of soot precursors, which consequently results in reduced engine-out emissions (Nerva et al., 2012). Nonetheless, it is also found that incomplete combustion may occur when vegetable oils with high viscosity and low cetane number (< 40) are used (Dagaut et al., 2007). Lower engine power output with the use of biodiesel instead of diesel has also been reported in the literature (Zhang et al., 2012). In view of this, better understanding of the fuel kinetics is essential in an effort to improve the biodiesel combustion and emissions performances. Both computational and experimental approaches are typically adopted to look into these complicated in-cylinder processes. However, Computational Fluid Dynamics (CFD) modelling approach is particularly favorable since its operating cost is usually much lower than the experimental approach. Besides, it is able to generate high-fidelity results with reasonable accuracy, depending

on the numerical models selected to optimize the complex computations during the simulations.

1.1.1 Biodiesel Fuel Kinetics

One of the most commonly used commercial biodiesel fuels in Western Europe is rapeseed methyl ester (RME) (Westbrook et al., 2011). It is derived through transesterification of rapeseed oil with methanol, which comprises 4.3 % methyl palmitate ($C_{17}H_{34}O_2$), 13.2 % methyl linolenate ($C_{19}H_{32}O_2$), 21.1 % methyl linoleate ($C_{19}H_{34}O_2$), 59.9 % methyl oleate ($C_{19}H_{36}O_2$) and 1.3 % methyl stearate ($C_{19}H_{38}O_2$) (Herbinet et al., 2010; Westbrook et al., 2011). Both methyl palmitate and methyl stearate are saturated methyl esters while the others are unsaturated methyl esters.

It is noted that biodiesel generally comprises long-carbon-chain methyl ester components (i.e. C_{14} to C_{22} esters) with numerous numbers of double bonds in the chain. Therefore, the chemical kinetics of the biodiesel combustion is very complicated. This poses a huge challenge for kinetic modelling. In view of the complexity of the kinetics of the actual biodiesel fuel, a “surrogate” model with simpler and well-characterised fuel compositions is commonly favourable instead to emulate the combustion behaviours of the actual biodiesel in the numerical modelling studies.

1.1.2 Kinetic Model Reduction

In general, the commercial biodiesel fuel contains hundreds or thousands of species. Thus, it is expected that the size of the kinetic model developed to reproduce the actual biodiesel fuel combustion behaviours is inevitably large. To date, the construction of a detailed model comprising all the actual biodiesel fuel constituents is yet to be accomplished owing to the limitations in computational resources and lack of fundamental knowledge of chemical kinetics. In spite of these, it is evident that better

model predictions can be achieved when a multi-component surrogate model is used. This subsequently leads to increment in the fuel chemistry size tremendously and it is unfeasible to apply them in CFD simulations due to its huge computational demand with greater possibility of code crash and divergence. Therefore, it is crucial to construct a compact representative for the actual biodiesel fuel for successful CFD computations with appropriate model accuracy.

1.2 Problem Statements

The fuel chemistries that represent the kinetics of the biodiesel fuels are too large and complicated for the investigation study of in-cylinder combustion and emission processes via CFD modelling approach. Apart from that, it is noted that more accurate simulations can be achieved if fuel compositions (e.g. percentage of saturated and unsaturated fatty acid methyl ester (FAME)) and cetane number of the kinetic model match those of the actual fuel, which is hard to be achieved through the use of a single-component kinetic model. Besides, some of the existing kinetic models are constructed for specific biodiesel feedstock and thus they are not suitable to be used as a representative for other feedstocks. Recognizing these limitations, development of a compact multi-component kinetic model with matching fuel compositions as the actual fuel is needed for successful CFD simulations of various biodiesel feedstocks.

1.3 Research Questions

Based on the problem statements depicted in Section 1.2, the following research questions for this project are raised:

- (i) What are the optimal fuel compositions and components that should be used to develop the biodiesel fuel kinetic models for successful CFD simulations under diesel-engine like conditions?

- (ii) How can the reduced kinetic model be used as a representative for various biodiesel feedstocks in multi-dimensional CFD applications?

1.4 Aim and Objectives

This study aims to address issues pertaining chemical kinetic modelling of biodiesel fuel combustion. The main objectives of this work are to:

- (i) develop a multi-component biodiesel fuel model which is applicable across a wide range of engine conditions;
- (ii) validate the derived biodiesel kinetic model in zero dimensional (0-D) kinetic simulations and two-dimensional (2-D) CFD spray combustion simulations; and
- (iii) investigate the applicability of the reduced model as a universal biodiesel fuel surrogate model for various biodiesel feed-stocks.

1.5 Scope and Limitations

The present work focuses on the development of a reduced chemical kinetic model for a biodiesel fuel surrogate, along with the associated model validation exercises with respect to the relevant currently-available experimental measurements under engine-like conditions. The compact model is formulated through a series of mechanism reduction practices based on a designated detailed chemical kinetic model for biodiesel fuel surrogate. Therefore, the developmental work here is constraint by the availability of the existing detailed models in the literature.

1.6 Outlines of the Thesis

The background of this research work along with the associated objectives and scope of the study is defined in Chapter 1. This is followed by a comprehensive literature review

on the developmental work of various kinetic models for the biodiesel fuel surrogate and various kinetic model reduction techniques in Chapter 2. Subsequently, the research methodology as well as the theoretical backgrounds of the numerical models applied in this study are presented in Chapter 3. In Chapter 4, the developmental work of the reduced biodiesel kinetic model is reported. On the other hand, the corresponding model validation exercises using 0-D and 2-D simulations are presented in Chapters 5 and 6, respectively. Following that, the applications of the reduced model as a generic surrogate model for different biodiesel feed-stocks are examined and the results are published in Chapter 7. Lastly, key conclusions derived from this research work are summarized in Chapter 8, together with some recommendations for further work.

CHAPTER 2: LITERATURE REVIEW

2.1 Introduction

In this chapter, overviews on the typical commercial biodiesel fuels used in both experimental and modelling studies are presented in Section 2.2. Following that, the literature reviews of current research work concerning the development of various chemical kinetic models for biodiesel combustion simulations as well as various kinetic model reduction approaches are depicted in Sections 2.3 and 2.4, respectively. Lastly, a summary of the literature reviews presented is provided in Section 2.5.

2.2 Overviews on Actual Biodiesel Fuels

Biodiesel is a renewable fuel comprising long-chain mono-alkyl esters that is derived from renewable feed-stocks such as vegetable oils and animal fats. Transesterification process is employed in the production of biodiesel through catalyzed reaction of the triglycerides presented in the vegetable oil or animal fat with the use of a monohydric alcohol (Meher et al., 2005). In general, biodiesel has a long hydrocarbon-chain structure with sixteen to nineteen carbon atoms attached to the methyl ester group (Herbinet et al., 2008). The average FAME compositions of various types of biodiesel fuels are presented in Table 2.1.

Table 2.1: Average FAME compositions of different biodiesel fuels (Mishra & Solanki, 2016).

Fuel	FAME Compositions (wt. %)							
	C12:0	C14:0	C16:0	C18:0	C18:1	C18:2	C18:3	C22:1
Rapeseed		1.5	1-4.7	1-3.5	13-38	9.5-22	1-10	40-64
Soybean			11	4	23	54	8	
Sunflower			6	5	29	58	1	1
Palm		1	45	4	39	11		
Coconut	44-51	13-18.5	7.7-10.5	1-3	5-8.2	1-2.6		

It is noted that these FAME components can be further divided into two categories, i.e. saturated and unsaturated FAME. The average saturated and unsaturated levels of the actual biodiesel fuels, such as RME, Soy Methyl Ester (SME), Sunflower Methyl Ester (SFME) and Palm Methyl Ester (PME), are depicted in Table 2.2.

Table 2.2: Percentage of saturated and unsaturated FAME in the actual biodiesel fuels by mass (Herbinet et al., 2008).

Fuel	Saturation Level (%)	Unsaturation Level (%)
RME	~6	~94
SME	~12	~88
SFME	~32	~68
PME	~48	~52

There are five saturated and unsaturated FAME which are typically found in most of the biodiesel fuels, namely methyl palmitate ($C_{17}H_{34}O_2$), methyl stearate ($C_{19}H_{36}O_2$), methyl oleate ($C_{19}H_{34}O_2$), methyl linoleate ($C_{19}H_{32}O_2$), as well as methyl linolenate ($C_{19}H_{30}O_2$). Among these, methyl palmitate and methyl stearate are the saturated FAME, while the rest are the unsaturated FAME which are characterised by the double bonds in their hydrocarbon chain. These are illustrated in Figure 2.1.

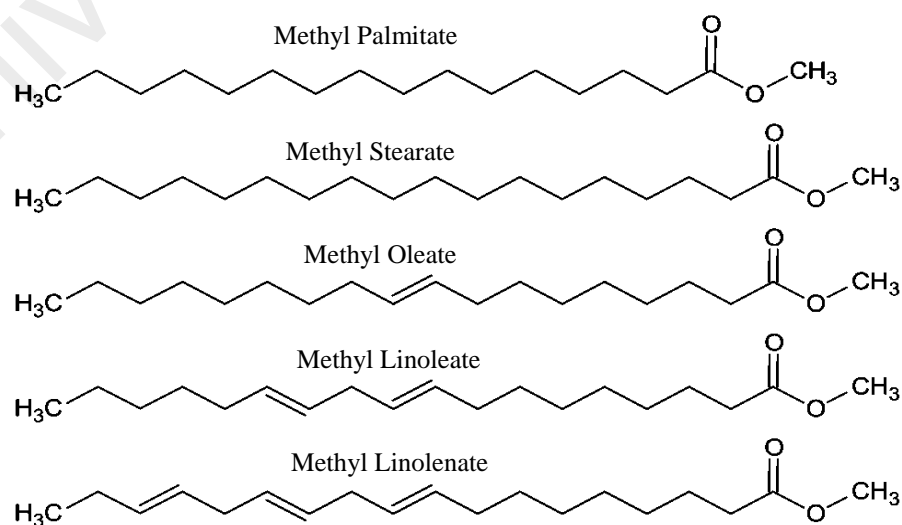


Figure 2.1: Hydrocarbon structures of the FAMEs (Bax et al., 2010).

It is reported that the double bonds presented in the hydrocarbon chain of the unsaturated FAMEs are accountable for the formation of soot precursors (Herbinet et al., 2010). The formation of resonantly stabilized radicals is promoted owing to the addition of radicals to the double bonds. It is noted that these resonantly stabilized radicals play an important role in the formation and growth of polycyclic aromatic hydrocarbons (PAH) which act as the soot precursors in combustion flames (Sinha et al., 2017).

Besides, the presence of double bonds has also influenced the fuel reactivities as certain low-temperature reactions are constrained. According to the experiments conducted by Zhang et al. (2009) in a motored CFR engine using C₉ FAME, the unsaturated esters are found to be less reactive as compared to the saturated esters. This can be attributed to the declined formation of 6-member and 7-member transition states during the oxidation of the unsaturated FAME.

On the other hand, the impacts of FAME compositions on the engine performance are investigated by Ruhul et al. (2016) using the experiment approach. The results obtained revealed that the increment in carbon chain length and saturation level of the FAME has led to the increment in the Cetane Number (CN) of the fuel. Similarly, the experimental studies of Zhu et al. (2016) have also demonstrated the correlation of molecular structure of FAME with the fuel combustion and emission characteristics. It is observed that the production of HC, CO and smoke increases with carbon chain length of FAME. The presence of double bonds of unsaturated FAME has resulted in higher CO and HC formation, with higher brake-specific fuel consumption than the saturated FAME.

Based on the experimental observations, it is found that both saturated and unsaturated FAMEs exhibit different fuel reactivities and ignition/emission behaviors. Hence, it is important to include both components during the construction of the kinetic models in order to successfully emulate the actual biodiesel fuel combustion and emission characteristics during the modelling studies.

2.3 Various Kinetic Models for Biodiesel Fuels

During the early kinetic studies of biodiesel fuel combustion, methyl butanoate (MB) has been extensively used as a surrogate model due to its simple alkyl structure and so its required computational power is lower. MB is a short-chain FAME with 4 carbon atoms attached to the methyl ester. As compared to the hydrocarbon structures of the actual biodiesel which usually contains 16 – 18 carbon atoms, the short-carbon-chain structure of MB is unable to reproduce the kinetic features of the oxidation of actual biodiesel fuels. Apart from this, MB is less reactive (Gaïl et al., 2008) with marginal negative temperature coefficient (NTC) regions as compared to the actual biodiesel fuels (Fisher et al., 2000; Gaïl et al., 2007; Mohamed Ismail et al., 2013).

In view of these, it is not favourable to use MB in the numerical modelling studies and surrogate models with long hydrocarbon chain surrogate model are preferred such as methyl hexanoate, methyl heptanoate, methyl octanoate and methyl decanoate (MD). Among these long-chain FAMEs, methyl hexanoate (Dayma et al., 2008; HadjAli et al., 2009) and MD (Diévar et al., 2012; Herbinet et al., 2011, 2008; Seshadri et al., 2009) are commonly selected as the representative as their fuel reactivities are similar to the actual biodiesel. The detailed models for these FAMEs generally consist of approximately 1,000 to 3,000 species, while the reduced models which are developed based on these detailed models usually contain more than 100 species (Diévar et al., 2012; Shi et al., 2010).

It is noted that the actual biodiesel fuel contains both saturated and unsaturated FAME, and thus surrogate model comprising these two components are suggested (Gaïl et al., 2008). Following that, a 301-species multi-component surrogate model consisting the saturated MB and unsaturated methyl(E)-2-butenate (MB2D) are generated (Gaïl et al., 2008). The presence of the additional double bond in MB2D has resulted in greater production of unsaturated species and soot precursors. Realizing the drawbacks of short-chain surrogate models, two detailed kinetic models to represent unsaturated FAME in

biodiesel are developed by Herbinet et al. (2010), namely methyl-5-decenoate (MD5D) and methyl-9-decenoate (MD9D). MD5D is found to have lower reactivity than MD9D and the influence of double bond in the unsaturated FAME on the reactivity level of biodiesel fuel is established.

Successively, multi-component surrogate model which combines MD with MD9D and n-heptane (An et al., 2014; Herbinet et al., 2010; Li et al., 2018; Luo et al., 2011) has become a popular choice as this integrated model provides the flexibility to achieve comparable physical and combustion properties with those of the actual biodiesels derived from different feed-stocks. In this way, the model compositions can be manipulated to match the configurations of various biodiesel fuels.

2.4 Kinetic Model Reduction

Sensitivity analysis is one of the conventional techniques used in model reduction in the earlier years. The approach is simple and straightforward. It is often applied to determine the impacts of the investigated parameters on the dynamic phenomena and it can be categorized based on the targeted studies, such as concentration sensitivity, reaction rate sensitivity and feature sensitivity (Rabitz et al., 1983). During the analysis, instantaneous quantitative error measurement of the numerical computations is provided. However, this technique involves huge computational time-cost in the post-processing. This is evident in a few numerical studies in the past years (Turányi et al., 1989; Turányi, 1990; Zheng et al., 2007). In the reduction work of Zheng et al. (2007), concentration sensitivity is computed using a Brute-force method which requires massive computational power to perform the iterative process. On the other hand, a sensitivity matrix is constructed to calculate the species production rate during the rate sensitivity analysis of Turányi et al. (1989). Despite its accurate predictions, high computational power is consumed as each eliminated species is validated one-by-one during the reduction

procedure. As a result of these limitations, sensitivity analysis is only applicable for reduction of small-sized kinetic models.

Jacobian-based methods (Massias & Diamantis, 1999; Turanyi, 1990; Valorani et al., 2006) are also among one of the conventional techniques used in kinetic model reduction. These approaches utilize Jacobian matrix to compute species coupling, whereby species which is strongly coupled with the target species is retained in the reduced model. Intrinsic Low-Dimensional Manifolds (ILDM) (Bongers et al, 2002; Correa et al., 2000; Maas & Pope, 1992) is one of the typical Jacobian-based reduction techniques that are widely used in the numerical studies. It is commonly employed to reduce the quantity of concentration variables from around 50-100 to only 1-3 (Correa et al., 2000). Nonetheless, numerical issues such as relaxation to unphysical negative concentrations as well as eigenvalues problems, are encountered during the computations. On the other hand, Bonger et al. (2002) has extended the novel ILDM method with diffusion, and it is called phase space ILDM (PS-ILDM). It is noted that diffusion is not taken into account during the development of the novel ILDM and hence the predictions are less accurate in regions where both chemistry and diffusion are significant. The approach has been successfully applied on a CO/H₂ kinetic model with greater accuracy in the flame predictions where both reaction and diffusion are significant. Besides, this method is also similar to the earlier flamelet-generated manifold method (FGM) developed by Van Oijen and de Goey (2002). FGM is more effective in applications related to laminar premixed flames since it is developed for premixed systems, whereas ILDM can be used in both non-premixed and partially premixed applications. Another Jacobian-based reduction method that is commonly used is the Computational Singular Perturbation (CSP) method (Lam & Goussis, 1994; Lu et al., 2001; Valorani & Goussis, 2001; Zagaris et al., 2004). This method is able to determine the steady-state species and the time scales for the consumption/production of species during combustion. A 4-step and a 10-step reduced

kinetic models are successfully developed to simulate the high-temperature oxidation process of H₂/air and CH₄/air in the modelling work of Lu et al. (2001). In spite of the advantages of ILDM and CSP, high demand of computational time and storage space are required. On top of that, these techniques involve selection of arbitrary threshold value for the Jacobian matrix and system-dependent knowledge is usually necessary.

Furthermore, Principle Component Analysis (PCA) (Brown et al., 1997; Vajda et al., 1985; Wold et al., 1987), which is developed based on the sensitivity analysis approach, is also among one of the conventional methods used in model reduction. The technique performs well in identifying redundant reactions and its accuracy depends on the reduction criterion selected for the reduction procedure. Similar to the other methods of sensitivity analysis, the PCA method requires computation of the sensitivity matrix. Thus, it is not suitable to be used for model reduction of large kinetic chemistries.

Owing to the limitations of the conventional reduction methods, the Directed Relation Graph (DRG)-based reduction techniques are formulated to handle large-scale kinetic models. These approaches are popular as the corresponding chemical analysis is straightforward and their application to kinetic modelling codes is simpler. A pre-determined numerical criterion is applied to identify the insignificant species and reactions with the use of various types of graph searching algorithms. The DRG method of Lu and Law (2005) has a similar approach with the Jacobian analysis (Tomlin et al., 1997), in which it resolves species coupling to filter out insignificant species during the reduction process. However, it does not require iterative process and it is able to determine all the important species in a single run. The time taken is linearly proportional to the number of edges in the graph. A universally specifiable threshold value normalised between 0 and 1 is applied during the DRG reduction process, which at the same time indicates the upper error bound for the reduced model. The application of DRG method on the detailed n-heptane and iso-octane models has successfully achieved overall species

reduction of about 66% - 73% (Curran et al., 1998, 2002). However, it is pointed out that the coupling coefficient adopted by DRG for error calculation is not directly related to an error measure (Pepiot & Pitsch, 2005). In addition, every selected species is equally important and all the other species which are strongly coupled to it must be retained, which may not be necessary.

In order to overcome the limitations of DRG, a generalised coupling coefficient based on error propagations is coupled into the novel DRG approach and it is called DRG with Error Propagation (DRGEP) (Pepiot & Pitsch, 2005). Error transmission from a species to the targets is taken into account and the selected species are no longer equally important. Species which is located far from the targets might be more significant than species which is directly linked to the targets. It is found that greater accuracy is achieved using the reduced model developed from DRGEP method as compared with that developed from the DRG method, when same number of species present in both models. Nonetheless, it is found that DRGEP is unable to identify the relations between species that have both fast rate of production and rate of consumption taking place simultaneously (Shi et al., 2010).

DRG aided Sensitivity Analysis (DRGASA) is an extended procedure of DRG (Sankaran et al, 2007; Zheng et al., 2007). Since DRG assumes upper-bound error propagation during the graph-searching process, size of the resulting reduced kinetic model is usually not nominal yet. Therefore, sensitivity analysis is integrated into DRG to maximize the reduction scale. Through the application of DRGASA reduction approach, a skeletal n-heptane kinetic model with 78 species which is previously developed from DRG method has been further reduced to only 55 species. Nevertheless, it is reported that DRGASA is unable to identify all the insignificant species as a result of species shielding effect (Niemeyer et al., 2010). The large-scale elimination of low-error unimportant species might induce a larger error than the allowable error during the

sensitivity analysis (Nagy & Turanyi, 2009). In view of the limitations of DRGEP and DRGASA, an integrated model reduction method is introduced by Niemeyer et al. (2010), namely DRG with Error Propagation and Sensitivity Analysis (DRGEPSA). The technique combines both DRGEP and DRGASA approaches, so the weaknesses of each method can then be overcome, and greater reduction scale can be achieved.

According to the modelling studies conducted by Poon (2016), the performance of the DRG, DRGASA, DRGEP, and DRGEPSA methods are evaluated in 0-D kinetic simulations based on their reduction scale in model size and computational time required. It is reported that the size of the reduced models formulated from these reduction techniques is not minimal yet for the multi-dimensional numerical modelling studies. Recognizing the limited reduction capability of these reduction approaches, an integrated five-stage reduction scheme is developed to cope with larger kinetic models for successful CFD simulations. The reduction scheme consists of five distinct stages, i.e. DRGEP using Dijkstra's algorithm, isomer lumping, reaction path analysis, DRG and adjustment of reaction rate constants. A reduced kinetic model for diesel with only 79 species is successfully derived from its detailed counterpart comprising thousands of species and elementary reactions. In overall, approximately 97 % reduction in total number of species as well as computational runtime in 0-D chemical kinetic simulations is achieved.

2.5 Chapter Conclusions

Based on the literature reviews of the biodiesel kinetic modelling studies, it is revealed that kinetic models with long-carbon-chain structures and combinations of saturated/unsaturated compositions are more appropriate to reproduce the kinetic behaviours of the actual biodiesel fuel. Thus, the detailed kinetic model of Herbinet et al. (2010) is chosen as the base model in this study. On the other hand, according to the literature reviews conducted for model reduction techniques, it is demonstrated that the

reduction scale is limited when only a single reduction method is applied in the reduction procedure, especially when dealing with large kinetic model. Hence, the reduction scheme of Poon (2006) which incorporates various reduction approaches is selected to perform model reduction in this study in order to achieve greatest extent of reduction.

University of Malaya

CHAPTER 3: RESEARCH METHODOLOGY

3.1 Introduction

In this chapter, the methodology used to conduct the research project is outlined in Section 3.2, along with the descriptions of the various numerical models applied in the model formulation and validation exercises. Next, the planned and actual timelines of the project are presented in Section 3.3. Lastly, the chapter conclusions are provided in Section 3.4.

3.2 Methodology

The initial phase of this project deals with the development of a compact kinetic model which matches the actual biodiesel fuel compositions using an integrated chemical kinetic mechanism reduction scheme (Poon, 2016). The descriptions of the detailed kinetic model as well as the mechanism reduction scheme are provided in Section 3.2.1 and Section 3.2.2, respectively.

The second phase of the project deals with model validations in 0-D and 2-D simulations. Extensive validations of the reduced model under multiple shock tube conditions are first performed in 0-D simulations. In this phase, the 0-D closed homogeneous batch reactor and the open perfectly-stirred reactor (PSR) models of CHEMKIN-PRO software are used. These models are described in Section 3.2.3. Upon completion of model validations in 0-D simulations, the newly formulated reduced kinetic model is further assessed in 2-D simulations and CFD sub-models are coupled into the CFD solver to simulate spray combustion in a constant volume combustion chamber fueled with biodiesel. The descriptions of the CFD sub-models are presented in Section 3.2.4.

The last phase of the project deals with the application of the reduced model as a universal fuel surrogate model for different biodiesel feed-stocks. The compositions of

the reduced model are varied according to the saturation/unsaturation levels in each fuel. Evaluations of the model with respect to the detailed counterpart in both 0-D kinetic and 2-D spray combustion simulations are carried out for each configuration. Detailed explanations of the saturated and unsaturated FAME can be found in Chapter 2. The flow chart of the research project is presented in Figure 3.1.

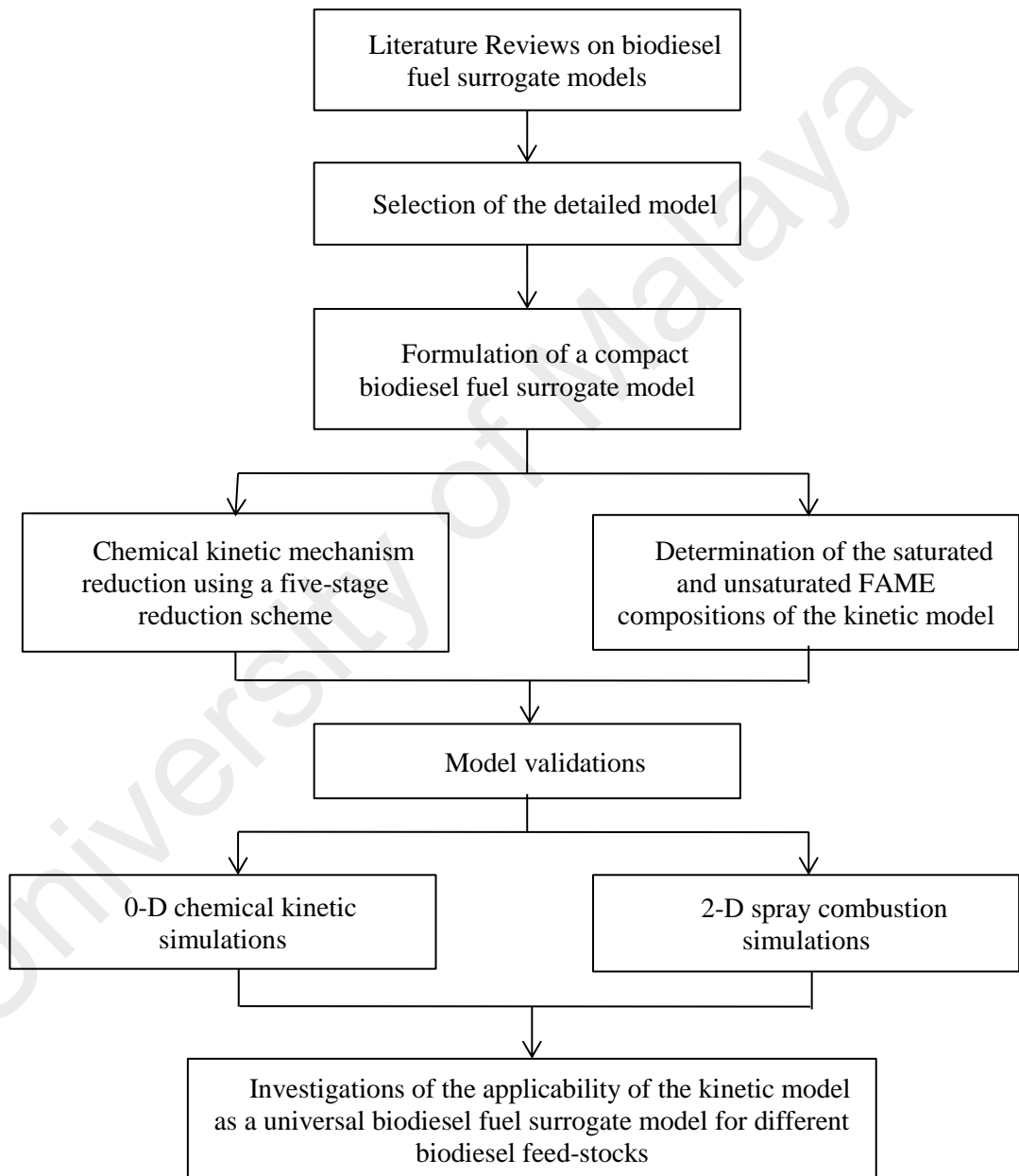


Figure 3.1: Flow chart of the research project.

3.2.1 Detailed Model of the Biodiesel Fuel

The surrogate model used to emulate the actual biodiesel fuel combustion in this study is the kinetic model developed by Herbinet et al. (2010). The model consists of three fuel components, namely methyl decanoate (MD), methyl-9-decenoate (MD9D) and n-heptane. MD is a saturated FAME and its ignition characteristics are comparable with those of the actual biodiesels. On the other hand, MD9D is an unsaturated FAME in which its double-bond's location is similar to that in methyl oleate as well as the first double-bond location in both methyl linoleate and methyl linolenate. The molecular structures of MD and MD9D are similar whereby both of them contain ten carbon atoms in the hydrocarbon chain. The only difference between them is MD9D possesses a double bond in the hydrocarbon chain, which is claimed to play an important role in the fuel reactivities. Apart from the presence of saturated and unsaturated FAMES in the surrogate model, n-heptane is also included in the detailed model to improve the model predictions and the integrated model has successfully replicated the oxidation of n-decane/methyl palmitate blend in a JSR (Dagaut et al., 2007). It is worth mentioning that the compositions of MD, MD9D and n-heptane can be varied to model the combustion behaviours of different biodiesel fuels. The detailed biodiesel fuel surrogate model consists of 3,299 species. Additionally, the nitrogen oxide (NO) sub-model derived from the GRI-MECH 2.11 (Bowman et al.) is also integrated into the kinetic model to predict thermal NO formation.

The input data file for the chemical kinetic model consists of all the elementary reactions and key chemical species which involve in the gas-phase chemistry systems, along with their important thermodynamic properties. On the other hand, the thermodynamic data file consists of all the physical properties of each chemical species and they are used to calculate the specific heats, enthalpies, and entropies of each species.

Besides, the Arrhenius rate parameters for each elementary reaction are provided and they are important in the computations of the rates of production and consumption of each species, which subsequently govern the chemical pathways of the fuel combustion process. These Arrhenius parameters are pre-exponential factor, A , temperature exponent, β and the activation energy, E_a . The temperature-dependent reaction rate constant, k , is thus obtained using these Arrhenius parameters, as depicted in Equation (3-1).

$$k = AT^\beta \exp\left(-\frac{E_a}{RT}\right) \quad (3-1)$$

whereby T is the temperature of the gas-phase combustible mixtures.

Here, it is noted that size of the detailed biodiesel fuel surrogate model is too large to be incorporated into multi-dimensional CFD simulations. Therefore, model reduction is desired for successful CFD simulations and the reduction scheme applied here is detailed in Section 3.2.2.

3.2.2 Five-Stage Chemical Kinetic Mechanism Reduction Scheme

A novel five-stage integrated chemical kinetic mechanism reduction scheme developed by Poon (2016) is applied to perform model reduction and ultimately obtain a compact surrogate model for the biodiesel fuel. The reduction scheme consists of five reduction stages, namely DRGEP using Dijkstra's algorithm, isomer lumping, reaction path analysis, DRG and adjustment of reaction rate constant. The flow chart of the reduction scheme is presented in Figure 3.2.

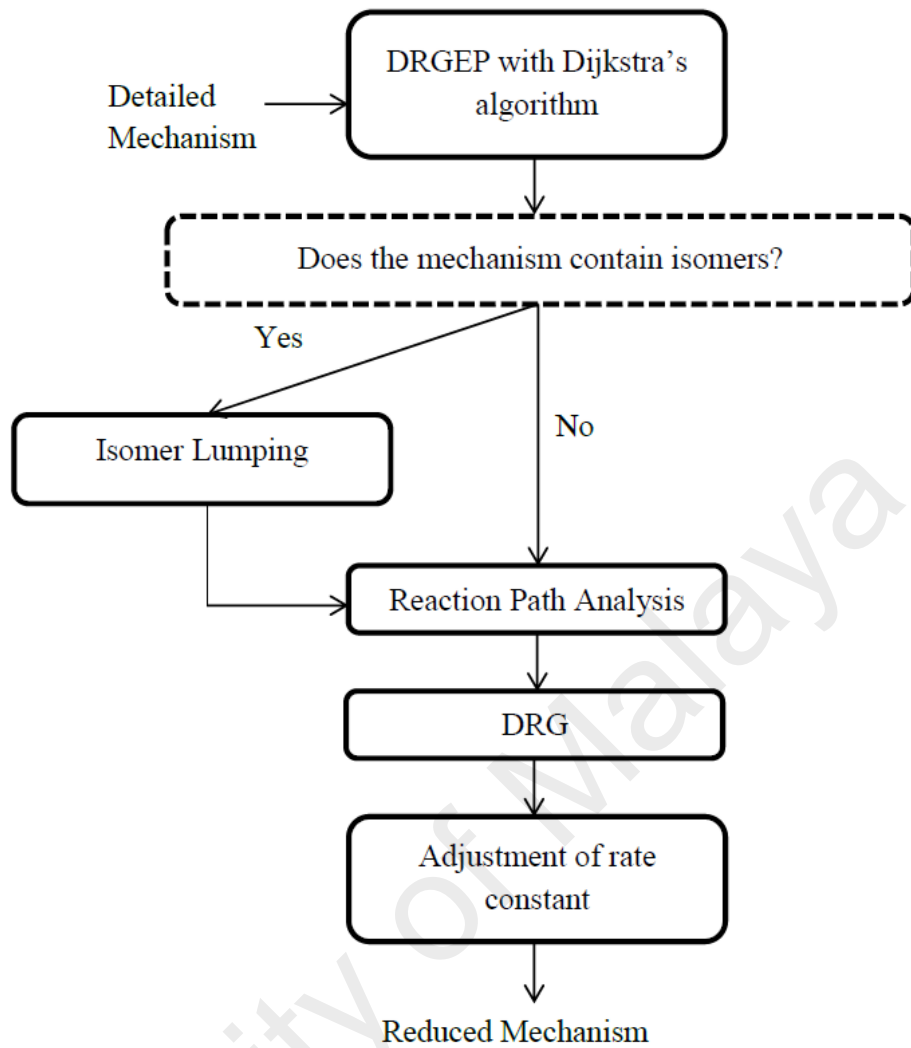


Figure 3.2: Five-stage integrated chemical kinetic mechanism reduction scheme (Poon, 2016).

First and foremost, DRGEP is performed to eliminate species with weak couplings among species using a generalised coupling coefficient, namely Direct Interaction Coefficient (DIC), based on error propagations (Pepiot & Pitsch, 2005). The species dependence on another is computed according to its impact on the overall species' production or consumption rate, as depicted in Equation (3-2).

$$DIC = \frac{|\sum_{j=1}^{N_R} v_{x,j} \omega_j \delta_y^j|}{\max\left(\underbrace{\sum_{j=1}^{N_R} \max(0, v_{x,j} \omega_j)}_{P_x}, \underbrace{\sum_{j=1}^{N_R} \max(0, -v_{x,j} \omega_j)}_{C_x}\right)} \quad (3-2)$$

P_x and C_x are the overall production and consumption rates of species x , respectively. N_R is the total amount of elementary reactions in the kinetic model. ω_j refers to the net reaction rate of the j^{th} elementary reaction, while ν_x refers to the stoichiometric coefficient of species x . δ_y^j is the participation of the another species, say species y , in the j^{th} elementary reaction. It is equal to unity if species y is involved in the j^{th} elementary reaction, whereas it is set to zero if there is no involvement. Subsequently, the maximum of all dependency pathways for all interrelated species with respect to the target species is computed. Here, a set of threshold value normalised between 0 and 1 is employed to screen out the insignificant species with weak species couplings. Dijkstra's algorithm is applied to calculate the reaction pathways, in which the shortest pathways from the target species to all other species is determined.

Next, isomer lumping is performed by grouping all the species with comparable thermodynamic and transport properties together into a specific representative lump. On top of that, species with very low concentration level, i.e. 1×10^{-10} mole/cm³, are eliminated during this reduction stage too. By doing so, a greater extent of reduction in the mechanism size is achieved. Following that, the major reaction pathways for the fuel oxidation process along with the corresponding species and elementary reactions are determined with the use of reaction path analyzer of CHEMKIN-PRO software. The influence of each reaction pathway to the net production rate of the joining species is assessed. On the other hand, the representative isomer for each specific lump is also determined here based on the reaction path widths which quantify the production rate of the connecting species. In general, species with high production rate is selected as the representative as compared to other isomers from the same isomer groups. Meanwhile, reactions of the connecting species which possess low normalised temperature A -factor sensitivity are removed during the reaction path analysis. This is performed carefully across all the operating conditions applied for the mechanism reduction process. Upon

completion of reaction path analysis, DRG is performed to eradicate all the unwanted species which have lost pathway connection to the target species.

Lastly, adjustment of reaction rate constant is performed as eliminations of species and elementary reactions from the detailed chemistries may cause deviations in the model predictions. Therefore, the *A*-factor value of Arrhenius parameters is adjusted such that the influence of the eliminated reactions is included in the Arrhenius rate constants of the retained reactions. Generally, reactions with high temperature *A*-factor sensitivity are selected for the adjustment. Further details of the integrated mechanism reduction scheme can be found in the previous work (Poon, 2016).

3.2.3 Closed Homogeneous Batch Reactor Model and JSR Model in 0-D Simulations

The closed homogeneous batch reactor model is a constant-volume closed system which does not possess any inlet or outlet flows. Therefore, there is no mass transfer between the system and the surroundings. On top of that, the reactor is also treated as an adiabatic system in which there is no heat exchange between the reactor and its surroundings. It is a transient system whereby the chemical state changes according to the production and destruction of species during the chemical reactions take place.

On the other hand, the JSR model is an open system which consists of a chamber connecting to the inlet and outlet ducts. The system is well-mixed to provide homogeneous mixtures and it runs at steady-state. The compositions within the reactor are assumed to be equivalent to the effluent stream, whereby the reactions occur at constant composition.

3.2.4 CFD Sub-Models in 2-D Simulations

3.2.4.1 Spray Breakup Model

Wave model is used to model the droplet breakup process as it is suitable for high speed injections. It is noted that the breakup of droplets comprises primary and secondary breakup. Here, the Kelvin- Helmholtz (KH) instability model is employed to model the primary breakup of fuel liquid core, while the KH model together with the Rayleigh-Taylor (RT) accelerative instabilities is employed to model the secondary breakup of individual fuel droplets. The KH breakup time, τ_{KH} is expressed by Equation (3-3):

$$\tau_{KH} = \frac{3.726B_1r}{\Omega_{KH}\Lambda_{KH}} \quad (3-3)$$

in which Ω_{KH} is the KH maximum growth rate, Λ_{KH} is the KH wavelength and r is the radius of newly-formed droplets. B_1 is the model breakup constant which governs the preliminary disturbance level during the liquid breakup process and the constant value generally ranges from 10 to 60. On the other hand, the RT breakup time, τ_{RT} is expressed by Equation (3-4):

$$\tau_{RT} = \frac{C_\tau}{\Omega_{RT}} \quad (3-4)$$

C_τ is associated to liquid core breakup and it has a value of 1 generally. C_3 usually ranges from 0.1 to 1 and it governs the child droplet size away from the breakup length which consequently affect the spray penetration length.

3.2.4.2 Turbulence Model

The turbulence interactions are simulated using the standard k-epsilon ($k-\epsilon$) model. The model is derived from the instantaneous Navier-Stokes equations and the expressions for k and ϵ are depicted in Equations (3-5) and (3-6), respectively. There are a few assumptions applied during the model derivation. First, the flow is treated as fully

turbulent. Second, the effects of molecular viscosity are unimportant. Therefore, the standard k - ε model is only applicable to fully-turbulent flows.

$$\frac{\delta}{\delta t}(\rho k) + \frac{\delta}{\delta x_i}(\rho k u_i) = \frac{\delta}{\delta x_j} \left[\left(\mu + \frac{\mu_t}{\sigma_k} \right) \frac{\delta k}{\delta x_j} \right] + G_k + G_b - \rho \varepsilon - Y_M + S_k \quad (3-5)$$

$$\frac{\delta}{\delta t}(\rho \varepsilon) + \frac{\delta}{\delta x_i}(\rho \varepsilon u_i) = \frac{\delta}{\delta x_j} \left[\left(\mu + \frac{\mu_t}{\sigma_\varepsilon} \right) \frac{\delta \varepsilon}{\delta x_j} \right] + C_{1\varepsilon} \frac{\varepsilon}{k} (G_k + C_{3\varepsilon} G_b) - C_{2\varepsilon} \rho \frac{\varepsilon^2}{k} + S_\varepsilon \quad (3-6)$$

ρ is the density, u is the velocity, and μ_t is the turbulent viscosity. G_k and G_b are the generation of turbulence kinetic energy due to mean velocity gradients and buoyancy, respectively. Y_M refers to the contribution of the fluctuating dilatation to the overall dissipation rate in compressible turbulence. $C_{1\varepsilon}$, $C_{2\varepsilon}$ and $C_{3\varepsilon}$ are the model constants which are by default set to 1.44, 1.92, and 0.09, respectively. On the other hand, σ_k and σ_ε are the turbulent Prandtl numbers for k and ε , which are set to 1 and 1.3, respectively. S_k and S_ε are the user-defined source terms.

3.2.4.3 Soot Model

The soot model applied in this work to capture the soot formation process is the multistep model by Leung et al. (1991). It is noted that the soot formation is a complicated process which can be generally divided into key phases such as soot inception, coagulation, surface growth and oxidation processes. Initially, the generation of soot precursor species as well as the soot surface growth species are calculated according to the gas-phase reactions. Here, C_2H_2 is set as the soot precursor/surface growth species. Next, the transport equations for soot particle number density, φ_N , and soot mass fraction, Y_{soot} , are computed with the use of the multistep model. The corresponding equations are:

$$\frac{\delta}{\delta t}(\rho \varphi_N) + \nabla \cdot (\rho \vec{v} \varphi_N) = \nabla \cdot \left(\frac{\mu_t}{S_{C_t}} \nabla \varphi_N \right) + \frac{1}{N_A} \frac{dN}{dt} \quad (3-7)$$

$$\frac{\delta}{\delta t}(\rho Y_{soot}) + \nabla \cdot (\rho \vec{v} Y_{soot}) = \nabla \cdot \left(\frac{\mu_t}{S_{C_t}} \nabla Y_{soot} \right) + \frac{1}{N_A} \frac{dM}{dt} \quad (3-8)$$

S_{C_t} is the turbulent Schmidt number while \vec{v} refers to the fluid velocity. N_A is the Avogadro number ($6.022 \times 10^{26} \text{ kmol}^{-1}$). dN/dt and dM/dt refer to the instantaneous and net production rate of soot particles, respectively.

3.3 Project Schedule

In this section, the breakdown of the projected and actual work schedules to complete the research project are depicted in Table 3.1. As aforementioned, the project is divided into three phases. The entire duration taken for the project completion is about six months.

Table 3.1: Project timelines.

Activities	Period (Months)	Month					
		1	2	3	4	5	6
Literature review	(Phase 1) 2	Planned					
		Actual					
Model formulation			Planned				
		Actual					
Model validations in 0-D kinetic simulations	(Phase 2) 2			Planned			
		Actual					
Model validations in 2-D spray combustion simulations					Planned		
		Actual					
Study of model applicability as a generic biodiesel fuel surrogate model	(Phase 3) 2					Planned	Planned
		Actual					Actual

 Planned
  Actual

From Table 3, it is observed that the overall project timelines are in accordance with the proposed schedules, except for the last phase of work in which early completion by a week is achieved.

3.4 Chapter Conclusions

The three phases of the entire project workflow are depicted in this chapter which include model development, validations and applications. Besides, the kinetic model as well as the reduction scheme applied to generate the reduced chemistries of the biodiesel fuel surrogate are described along with the governing equations used in the CFD simulations. Finally, both the projected and actual timelines of the research project are presented and discussed. In overall, the first two phases of the research project are completed according to the proposed work schedules, while the completion time of the third phase of work is brought forward by one week.

University of Malaysia

CHAPTER 4: BIODIESEL FUEL SURROGATE MODEL FORMULATION

4.1 Introduction

In this chapter, the procedures to formulate the reduced kinetic model is presented. Firstly, the fuel constituents of the surrogate model along with the respective composition used to represent the actual RME biodiesel are introduced in Section 4.2. Following that, the operating conditions applied during the model reduction process are depicted in Section 4.3. The detailed descriptions of the developmental work of the reduced kinetic model are then presented in Section 4.4. In the last section, the key findings of this chapter are highlighted.

4.2 Fuel Constituents

The compositions of the reduced model are determined based on the actual composition range of RME (Westbrook et al., 2011), i.e. approximately 6 % saturated FAME and 94 % unsaturated FAME. As aforementioned in Chapter 2, the detailed kinetic model which is selected to represent the actual RME biodiesel consists of three main components, namely MD, MD9D and n-C₇H₁₆. MD is chosen as a representative for the saturated component of RME owing to its similar ignition times and reactivities to real biodiesel (Herbiset et al., 2010). Meanwhile, MD9D is chosen as a representative for the unsaturated component of RME owing to its matching double-bond location with that in methyl oleate as well as the first double bond in methyl linoleate and methyl linolenate (Herbiset et al., 2010). The molecular structures of MD and MD9D are basically alike except the presence of a double bond in the hydrocarbon chain of MD9D. n-Heptane is included in the surrogate model in order to achieve compositional match with that of the actual biodiesel fuel in terms of the number of carbon and oxygen atoms presented in the fuel. In this study, the composition of n-C₇H₁₆ in the surrogate model is fixed at 50 % by mass. This is set according to the configurations used in the experimental work of Dagaut

et al. (2007) on RME oxidation in a JSR under dilute conditions. Subsequently, the remaining 50 % of the surrogate fuel compositions is then divided according to the saturated and unsaturated FAME percentages presented in the actual fuel.

4.3 Operating Conditions

In this work, the reduced kinetic model is developed based on a wide range of auto-ignition and JSR conditions, which serve as the data source for the model reduction. The operating conditions are depicted in Table 4.1. Here, the operating conditions selected are essentially the typical in-cylinder parameters for main fuel injections in a light-duty (Le & Kook, 2015), direct-injection diesel engine. Accordingly, the reduction procedure is conducted using the five-stage chemical kinetic mechanism reduction scheme, as described in Chapter 3. Closed homogeneous batch reactor and PSR models of CHEMKIN-PRO software are used.

Table 4.1: Operating conditions applied during mechanism reduction process.

Parameters		Values
(a) Auto-ignition	Equivalence ratio, Φ (-)	0.5, 1.0, 2.0
	Pressure, P (bar)	40, 60, 80
	Temperature, T (K)	650 K – 1350 K
(b) JSR	Equivalence ratio, Φ (-)	0.5, 1.0, 2.0
	Pressure, P (bar)	40, 60, 80
	Residence time, t_R (s)	1

4.4 Developmental Procedures of the Reduced Model

The kinetic model reduction procedures are performed using an integrated chemical kinetic mechanism scheme developed by Poon (2016), as described in Chapter 3. It consists of five phases, i.e. DRGEP, isomer lumping, reaction path analysis, DRG, and adjustment of reaction rate constants. The implementations of each reduction stage to

formulate the reduced biodiesel fuel surrogate model are further elaborated in Sections 4.4.1 to 4.4.5, respectively.

4.4.1 DRGEP

Firstly, DRGEP reduction with Dijkstra's algorithm is carried out as the first step of the model reduction process. Both auto-ignition and JSR conditions are designated as the data source for model reduction. As mentioned in the previous chapter, key intermediate and emission species such as CO, CO₂, HCO, HO₂, H₂O₂, H₂, and N₂ are chosen as the target species for the reduction exercise. This allows greater extension of reduction with higher accuracy, which ensures important species and reactions involving in the oxidation and chain-branching processes are not neglected during the elimination procedure. Consequently, a 463-species reduced model are generated upon successfully application of the DGREP reduction procedure.

4.4.2 Isomer Lumping

Following that, lumping of species with comparable thermodynamic and transport properties are performed. This permits greater reduction scale to be achieved. Meanwhile, isomers with concentration of 1×10^{-10} mole/cm³ are also eliminated during this reduction phase. It is found that the concentration level of these removed species is very low and hence does not place any significant effects on the fuel combustion process. Some examples of the isomers presented in the detailed model are provided in Table 4.2.

Table 4.2: Examples of isomers in the detailed kinetic model.

Lump(s)	Isomers
MD	MD2j, MD3j, MD4j, MD5j, MD6j, MD7j, MD8j, MD9j
MD9D	MD9D2j, MD9D3j, MD9D4j, MD9D5j, MD9D6j, MD9D7j, MD9D8j
MB	MB2j, MB3j, MB4j

4.4.3 Reaction Path Analysis

The next phase of the reduction procedure is the reaction path analysis. Here, the reaction path analyzer of CHEMKIN-PRO software is employed to assess the key reaction pathways during the fuel oxidation process. One of the examples of the major reaction pathways during the fuel oxidation process is presented in Figure 4.1.

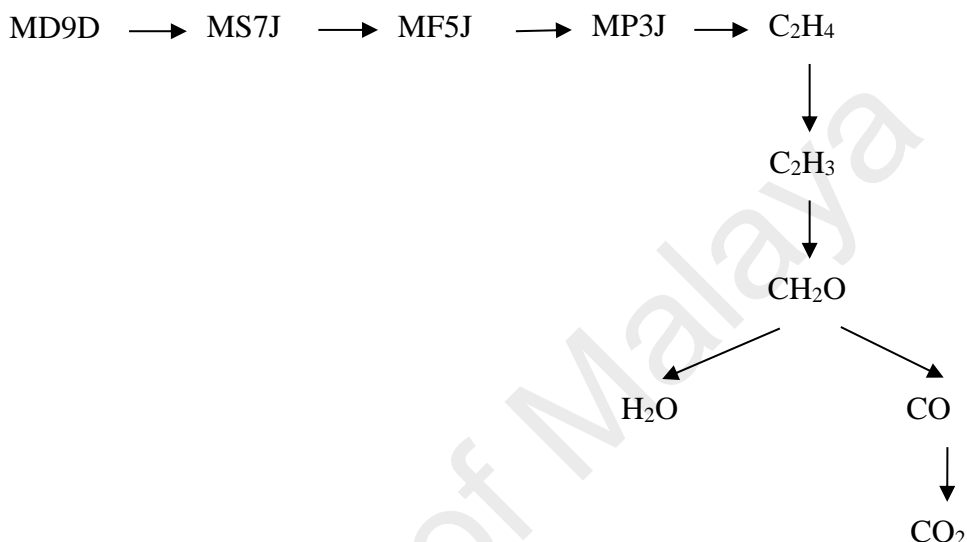


Figure 4.1: Example of one of the key reaction paths during fuel oxidation process.

On the other hand, it is found that fuel generally undergoes thermal decompositions under fuel-rich conditions. Meanwhile, H-atom abstractions on the fuel by OH, H and O radicals are more prevalent under fuel-lean conditions. For stoichiometric conditions, H-atom abstractions are more dominant at low temperature, while thermal decompositions of the fuel are more significant at high temperature and the significance increases with temperature.

4.4.4 DRG

Upon completion of reaction path analysis, DRG method is performed. Here, the threshold value is set to unity. The reason of doing so is to filter out all the species which

have lost pathway connection to the key species after isomer lumping and reaction path analysis.

4.4.5 Adjustment of Reaction Rate Constants

Appropriate adjustment of the *A*-factor constants of Arrhenius parameters (Brakora et al., 2011; Tao et al., 2007; Vishwanathan & Reitz, 2009) is next carried out. As large-scale species elimination from the detailed model may deteriorate the ID and species concentration predictions, optimisation of the *A*-factor is often used such that the influence of the eliminated reactions is included in the Arrhenius rate constants of the retained reactions. The comparison of the original and optimised *A*-factor values of Arrhenius parameters is demonstrated in Table 4.4. The *A*-factor values for reactions (R1) and (R5) are increased by one order of magnitude in order to improve the ID and fuel concentration predictions throughout all temperature regimes. *A*-factor values for reactions (R2), (R3) and (R4) are also adjusted to improve the ID predictions at intermediate-temperature regimes (i.e. $850 \text{ K} \leq T \leq 1050 \text{ K}$). As a result of the reduction procedures, a reduced model with only 84 species with 264 elementary reactions are successfully generated.

Table 4.3: Comparison of the original and adjusted *A*-factor values of Arrhenius parameters.

Reactions	A-factor values	
	Original	Adjusted
(R1) MD + OH = MD6J + H ₂ O	4.67E+07	4.67E+08
(R2) NC ₃ H ₇ + MS6D = MD6J	8.80E+03	8.80E+04
(R3) MD9D6J = C ₃ H ₅ -A + MS6D	3.31E+13	1.31E+14
(R4) C ₇ H ₁₄ OOH ₂ -4O ₂ = NC ₇ KET24 + OH	1.25E+10	1.25E+09
(R5) MD9D + OH = MD9D6J + H ₂ O	4.67E+07	4.67E+08

4.5 Chapter Conclusions

The application of the five-stage integrated reduction scheme has contributed to approximately 97.5 % reduction in the mechanism size in comparison to that of its detailed counterpart. The final reduced chemistries consist of 84 species with 264 elementary reactions. Consequently, the reduced model is thus applied in both 0-D and 2-D simulations for a series of model validation exercises. These are discussed in the following chapters.

University of Malaya

CHAPTER 5: MODEL VALIDATIONS IN 0-D CHEMICAL KINETIC SIMULATIONS

5.1 Introduction

Upon successful kinetic model formulation in Chapter 4, extensive validation exercise of the reduced model in 0-D chemical kinetic simulations are then performed and the computational results are presented in this chapter. The operating conditions applied here are first depicted in Section 5.2. Subsequently, the validation results with respect to the detailed model under both auto-ignition and JSR conditions are reported in Sections 5.3 and 5.4, respectively. Besides, the simulation results predicted by the reduced model are also compared with a set of experimental data of RME oxidation in a JSR in Section 5.5. Lastly, concluding remarks are made in Section 5.6 to summarize the findings obtained.

5.2 Operating Conditions

In this chapter, closed homogeneous batch reactor and PSR models of CHEMKIN-PRO software are used to perform model validations of the reduced kinetic model in 0-D chemical kinetic simulations. The operating conditions applied in these simulations are depicted in Table 5.1.

Table 5.1: Operating conditions for model validations in 0-D simulations.

Validation Parameters		Values
(a) Auto-ignition Conditions	Φ	0.5, 1.0, 2.0
	P	40, 60, 80 bar
	T	650 K – 1350 K
(b) JSR Conditions	Φ	0.5, 1.0, 2.0
	P	40, 60, 80 bar
	t_R	1 s
(c) JSR Experimental Measurements (Dagaut et al., 2007)	Φ	1.5
	P	1 atm
	t_R	0.1 s

5.3 Validations against detailed model under auto-ignition Conditions

First, the IDs calculated by the reduced model as well as its detailed counterpart are compared in this validation exercise. The results are shown in Figure 5.1. It is observed that good agreement is achieved between the calculated IDs by the reduced and detailed models, with maximum deviation maintained to within 40 %. This is acceptable as the error tolerance for ID comparisons against the detailed counterpart usually ranges from 30 – 50 % for large-scale mechanism reduction (Brakora et al., 2011; Luo et al., 2012; Niemeyer et al., 2010; Yang et al., 2012).

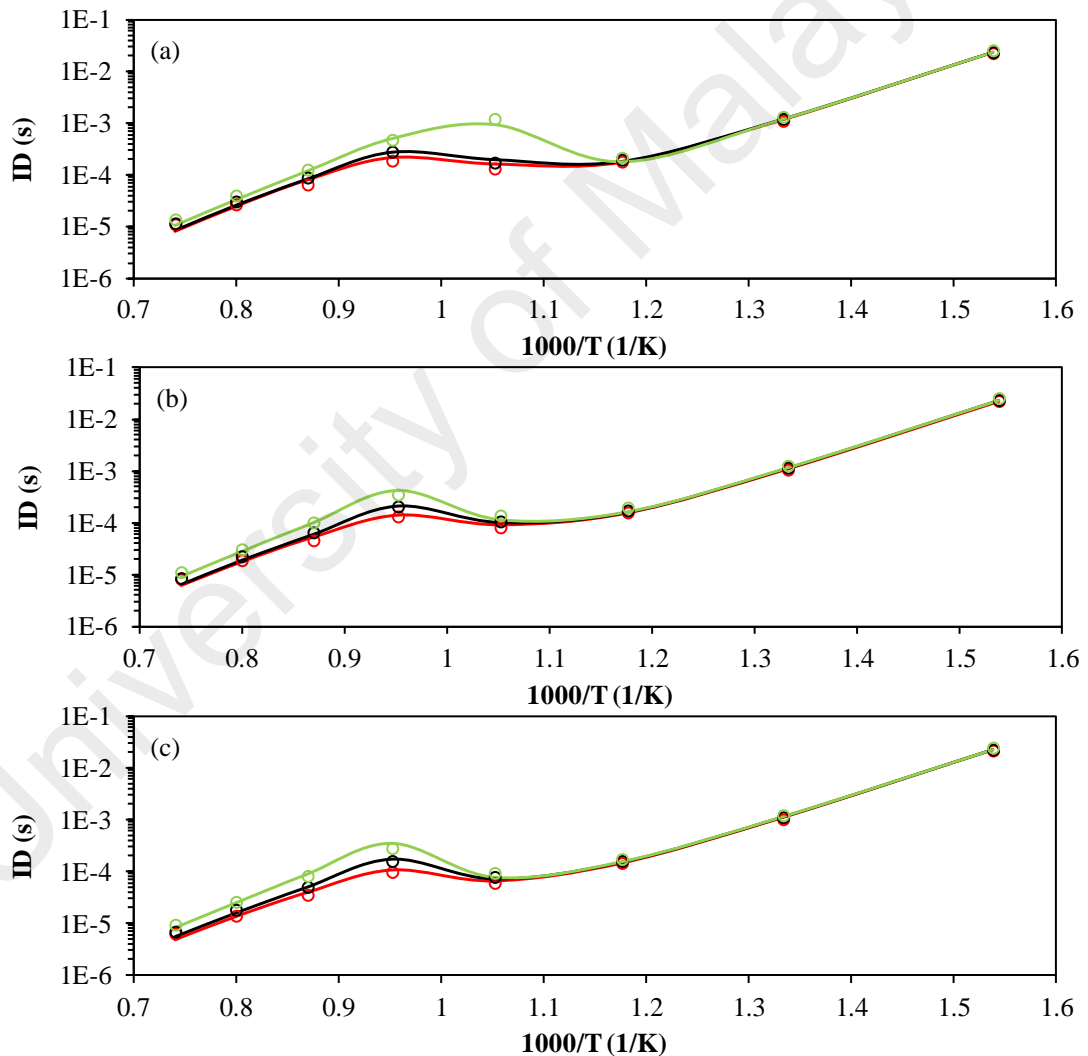


Figure 5.1: Comparisons of the IDs computed by the reduced (solid lines) and detailed (symbols) models under auto-ignition conditions at initial pressures of (a) 40 bar, (b) 60 bar, (c) 80 bar, Φ of 0.5 (green), 1 (black), 2 (red), over a temperature range of 650 K – 1350 K.

In addition, validations against the computed species concentration profiles by the detailed model are also performed in this section. The results are shown in Figure 5.2.

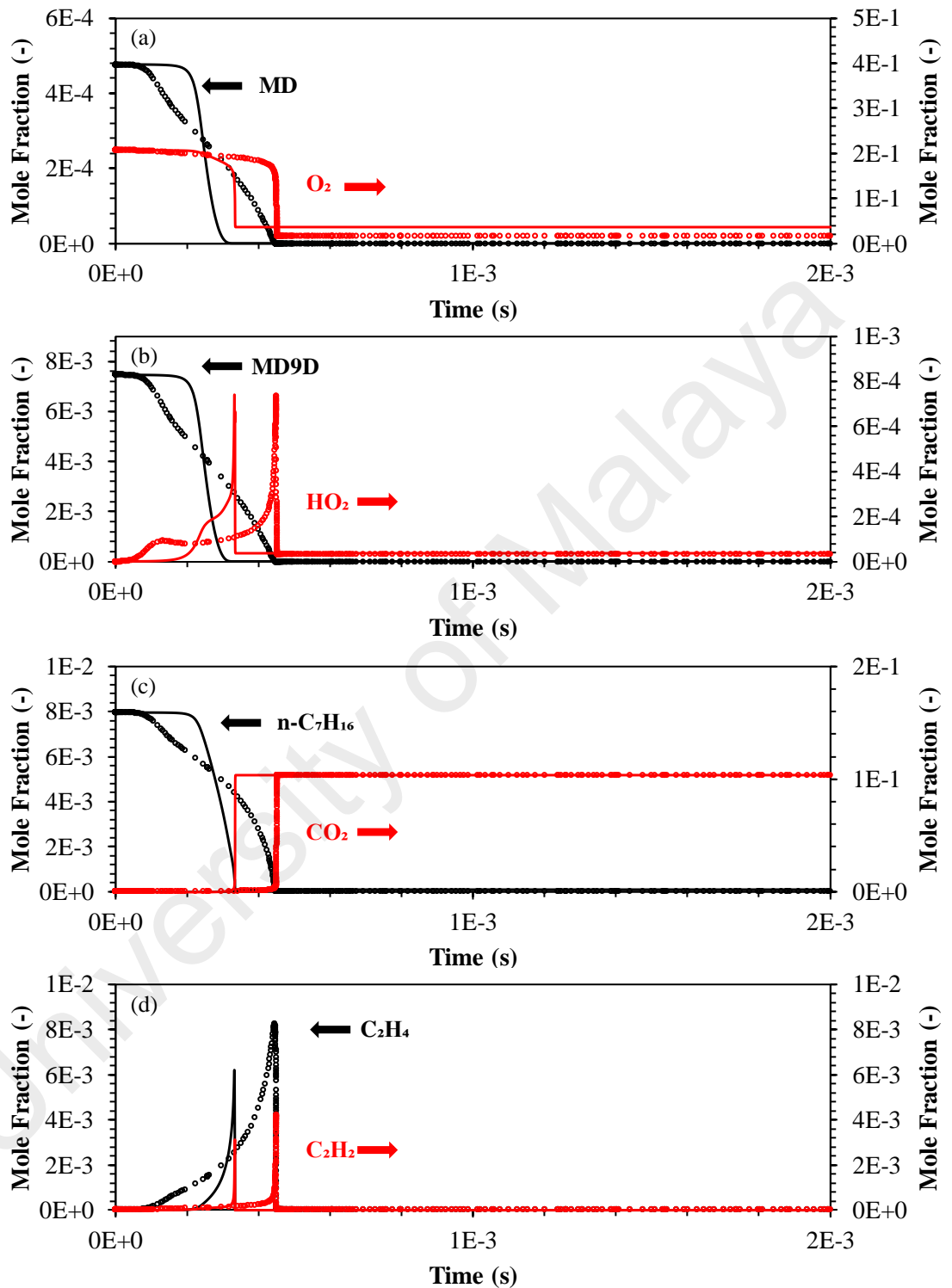


Figure 5.2: Comparisons of the computed species profiles by the reduced (solid lines) and detailed (symbols) models under auto-ignition conditions at initial pressure of 60 bar, Φ of 1, and temperature of 950 K.

In this study, only the computations for Φ of 1 and initial pressure of 60 bar are presented since similar species temporal evolution trends are obtained for other operating conditions stated in Table 5.1. The species evaluated here are including reactant species (MD, MD9D, n-C₇H₁₆, O₂), intermediate species (HO₂, C₂H₂, C₂H₄) and product species (CO₂).

Referring to the results shown in Figure 5.2, it is demonstrated that the overall species evolution trends computed by the reduced model are comparable with those of the detailed model, including the species concentration predictions at steady-state conditions. However, a small variance in the onset of species formation or decomposition are observed between the model calculations. This can be attributed to the variation in ID predictions using the reduced and detailed models, as shown in Figure 5.1. Therefore, the commencements of the species formation or decomposition process are consistent with the corresponding ID timings computed for the targeted species.

5.4 Validations against detailed model under JSR Conditions

In this section, model validations are carried out for fuel oxidation under JSR conditions, as described in Section 5.2. Here, the computed concentration profiles by the reduced kinetic model for important reactant species (i.e. MD, MD9D, n-C₇H₁₆, O₂), intermediate species (i.e. OH, HO₂, C₂H₂) and product species (i.e. CO₂) are compared with the computational results of the detailed counterpart. Similar to the previous section, only results of the species profiles at initial pressure of 60 bar and Φ of 1 are presented since the species concentration evolution trends are comparable for Φ of 0.5 and 2. The validation results are demonstrated in Figure 5.3.

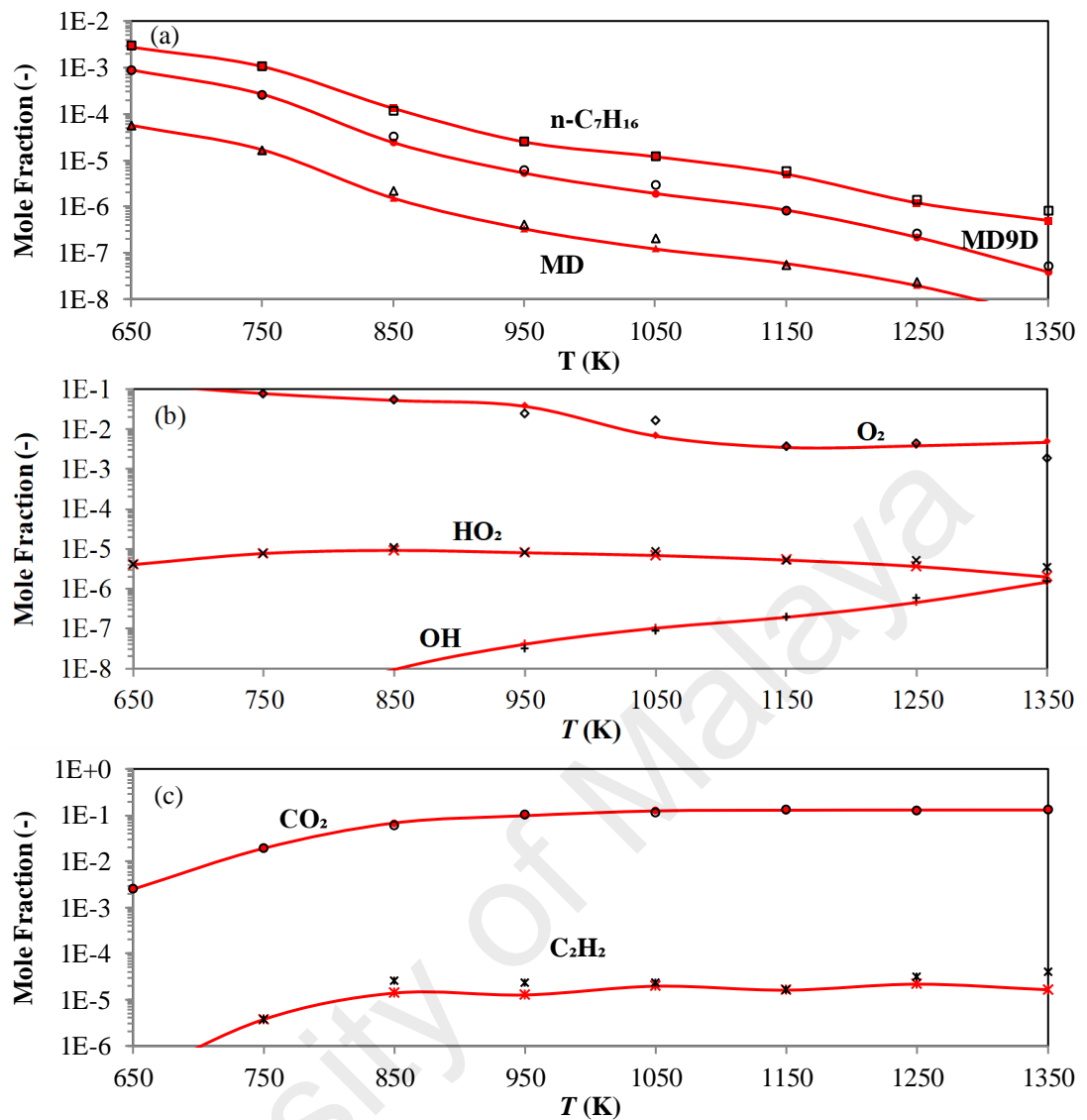


Figure 5.3: Comparisons of the computed species mole fractions by the reduced (solid lines) and detailed (symbols) models under JSR conditions at pressure of 60 bar, Φ of 1, and t_R of 0.1 s over a temperature range of 650 K – 1350 K.

Referring to Figure 5.3, it is observed that the reactivities of the different fuel components, namely MD, MD9D and $n-C_7H_{16}$, computed by the reduced model are comparable with those of the detailed model. In overall, the species profile trends predicted by the reduced model agree reasonably well with those of the detailed model throughout the tested conditions.

5.5 Validations against JSR Experimental Measurements

In addition, the reduced model is further validated with respect to a set of experimental measurements of key species concentrations produced from RME oxidation (Dagaut et al., 2007). The experiment was conducted in a fused-silica JSR operating at fixed residence time, t_R , of 0.1 s, Φ of 1.5 and pressure of 1 atm over a temperature range of 900 K – 1400 K. It is worth-mentioning that Φ of 1.5 is selected for this validation exercise as soot is mainly produced under fuel-rich conditions. Additionally, fuel-oxygen mixtures consisting high purity oxygen (99.995 % pure) and 0.05 % mole of RME fuel (which is highly diluted by a nitrogen flow of 100 L/h) are used in the experiment in order to obtain a steady-state operation with minimized temperature gradients inside the reactor (Dagaut et al., 2007).

On the other hand, a few gas chromatographs (GC) were employed to measure the species mole fractions. The GCs are equipped with capillary columns (Poraplot-U, Molecular Sieve-5A, DB-5ms, Plot Al₂O₃/KCl, Carboplot-P7), thermal conductivity detector and flame ionization detector. Meanwhile, chromatography / mass spectrometry (GC/MS) analysis was applied to identify different compounds within the test samples with the use of an ion trap detector (GC/ MS Varian Saturn) or a quadrupole (GC/MS Varian 1200) operating in electron impact ionization mode (70 eV). It is reported that the accuracy of the measured species mole fractions is approximately ± 10 % while the uncertainty on the experimental temperature is about ± 5 K (Dagaut et al., 2007).

Here, the key species selected for the validation exercise are important intermediate species (i.e. C₃H₆, CH₄, C₂H₄) and product species (CO, CO₂). It is noted that C₂H₄ is an important species which is highly associated with the production of soot precursor. Generally, C₂H₂ is commonly designated as a soot precursor species in many numerical simulations. Nonetheless, as measurements for C₂H₂ mole fractions are absent in the experiment, it is reasonable to use the measured data of C₂H₄ mole fractions for this

validation exercise. As such, this will aid in the subsequent multi-dimensional CFD simulations to predict the soot formation.

The validation results are shown in Figure 5.4. Here, the computations of the detailed model are also included so that direct comparisons between the predictions by the reduced and detailed models can be made.

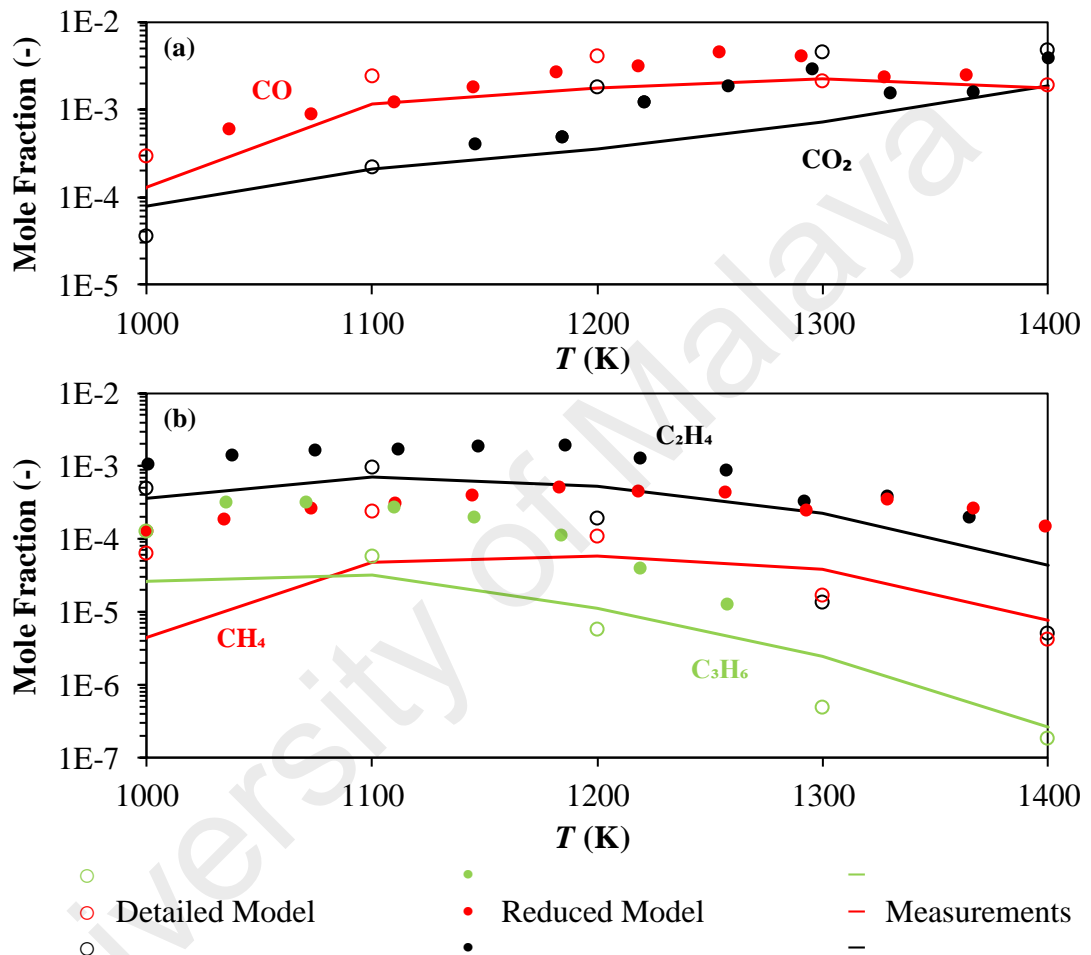


Figure 5.4: Comparisons of the computed and experimental species mole fractions of (a) CO, CO₂, and (b) CH₄, C₂H₄, C₃H₆ obtained from RME oxidation in a JSR.

Based on the results depicted in Figure 5.4, the kinetic modelling is found to be able to describe the experimental measurements reasonably well. The overall experimental species temporal evolution trends are fairly reproduced by the reduced model. Good agreement is also achieved between the calculations by both reduced and detailed model across the temperature range. The deviations between the model predictions can be

attributed to the elimination of some alkyl and alkyl-ester radicals during the model reduction process. Apart from these, it is worth-mentioning that improvements as high as one order of magnitude on the absolute values in the predictions of C_2H_4 mole fraction by the reduced model are achieved, in comparison to the computations by the detailed model. This will thus aid in enhancing the accuracy of the soot formation predictions in the successive modelling studies. In general, the species profiles predicted by the reduced model are consistent with the experimental data in this study, in spite of the variations on absolute values.

5.6 Chapter Conclusions

In this chapter, it is demonstrated that the reduced kinetic model is able to reproduce the overall ID and species profile trends of the corresponding detailed model with reasonable agreement and consistency. Besides, the temporal evolution trends of the measured species concentrations in a JSR are also well captured by the reduced model. Therefore, the validation results obtained here is deemed acceptable in view of its simplified fuel chemistries.

CHAPTER 6: MODEL VALIDATIONS IN 2-D SPRAY COMBUSTION SIMULATIONS

6.1 Introduction

In this chapter, the fidelity of the reduced biodiesel fuel surrogate model is further tested in 2-D spray combustion simulations. The numerical setups together with the computational mesh applied in the modelling studies are first described in Section 6.2. Following that, both non-reacting and reacting fuel spray conditions are applied accordingly to assess the model predictions in fuel spray behaviors as well as combustion /emission behaviors in Sections 6.3 and 6.4, respectively. Lastly, a summary on the simulation work presented in this chapter is provided in Section 6.5.

6.2 Model Formulations

In this chapter, the reduced kinetic model is further evaluated in SME fuel spray combustion phenomena with respect to the measured data obtained from the experiments conducted by Nerva et al. (2012). The corresponding experimental setups are described in Section 6.2.1. On the other hand, the numerical model configurations used in these constant-volume spray combustion simulations are depicted in Section 6.2.2.

6.2.1 Experimental Setups

The spray combustion experiment performed by Nerva et al. (2012) was conducted using a set of experimental apparatus comprising a constant-volume combustion vessel, high-pressure fuel injection system, an imaging system, as well as a data acquisition and control system (Siebers, 1998).

The constant-volume combustion vessel has a cubical shape with dimensions of 108 mm x 108 mm x 108 mm, as illustrated in Figure 6.1. It has a high-pressure capability of 35 MPa and it is equipped with optical access facility which permits line-of-sight and

orthogonal view for optical diagnostics. Two spark plugs and a mixing fan are mounted on the top wall of the vessel. The spark plugs are used to produce an inert high-temperature and high-pressure ambient in the combustion vessel prior to the fuel injection process; while the mixing fan is used to maintain uniform gas temperature distribution within the vessel.

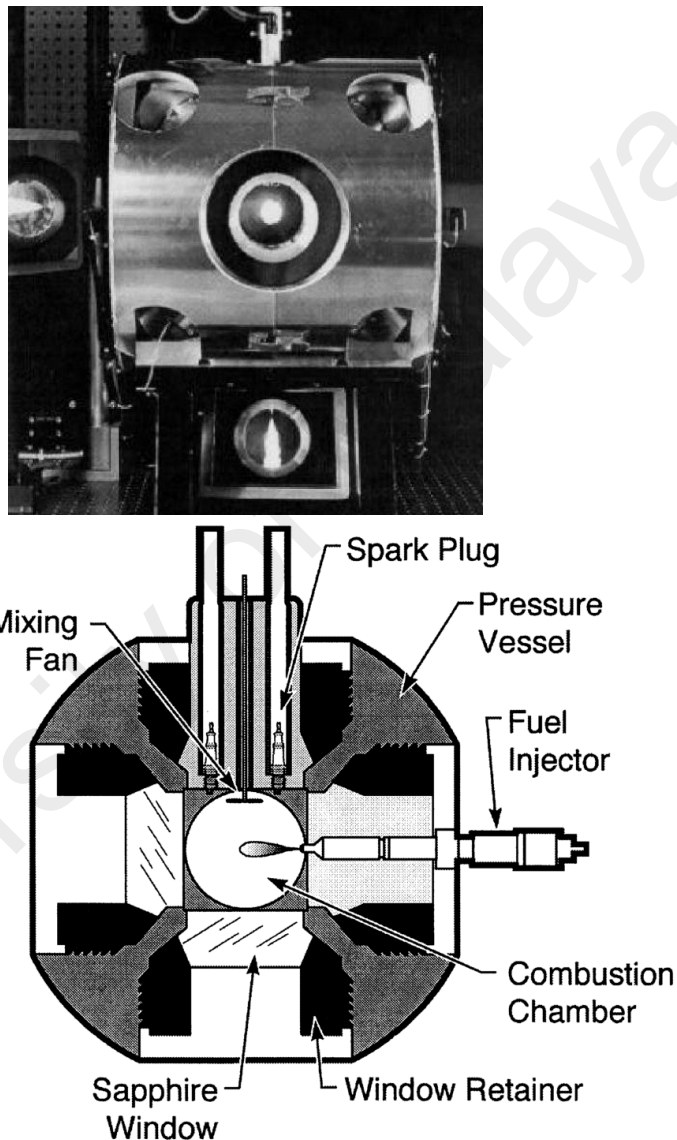


Figure 6.1: Photograph (top) and a schematic cross-section (bottom) of the constant-volume combustion vessel (Siebers, 1998).

Fuel is delivered by a single-hole injector with axial nozzle, which is located at one of the walls of the combustion chamber with horizontal mounting orientation. The Spray A operating conditions by Engine Combustion Network are applied for the fuel injection.

Details of the fuel injector characteristics and the experimental operating conditions are provided in Table 6.1 and Table 6.2, respectively.

Table 6.1: Fuel injector characteristics.

Type	Bosch common rail
Nozzle	Single hole, KS1.5/86, Min-sac type
Nozzle Diameter (μm)	(nominal) 90 / (measured) 90.8
Orifice Diameter (mm)	0.09
Injection Pressure (MPa)	150
Injection Duration (ms)	7
Discharge Coefficient	0.94
Fuel Temperature (K)	363

Table 6.2: Experimental operating conditions under reacting and non-reacting ambient conditions. (Nerva et al., 2012; Siebers, 1998).

Ambient temperature (K)	900 / 1000
Ambient pressure (MPa)	6.0 / 6.7
Ambient density (kg/m^3)	22.8
Ambient velocity	Near-quiescent, less than 1 m/s
Ambient oxygen (% by volume)	15% O ₂ (Reacting) 0% O ₂ (Non-reacting)
Ambient compositions (% by volume)	15% O ₂ , 6.23% CO ₂ , 3.62% H ₂ O, 75.15% N ₂ (reacting) 0% O ₂ , 6.52% CO ₂ , 3.77% H ₂ O, 89.71% N ₂ (Non-reacting)

Besides, an imaging system shown in Figure 6.2 is used to collect images of the fuel sprays. Mie-scattering and Schlieren high-speed imaging are employed concurrently to characterize the fuel mixing processes under inert and reactive settings. The spray liquid and vapour phase images are captured, and their associated spatial and temporal relationship can thus be assessed. On the other hand, OH chemiluminescence, planar laser-induced incandescence (PLII), and laser extinction are used simultaneously to quantify soot formation in the experiment.

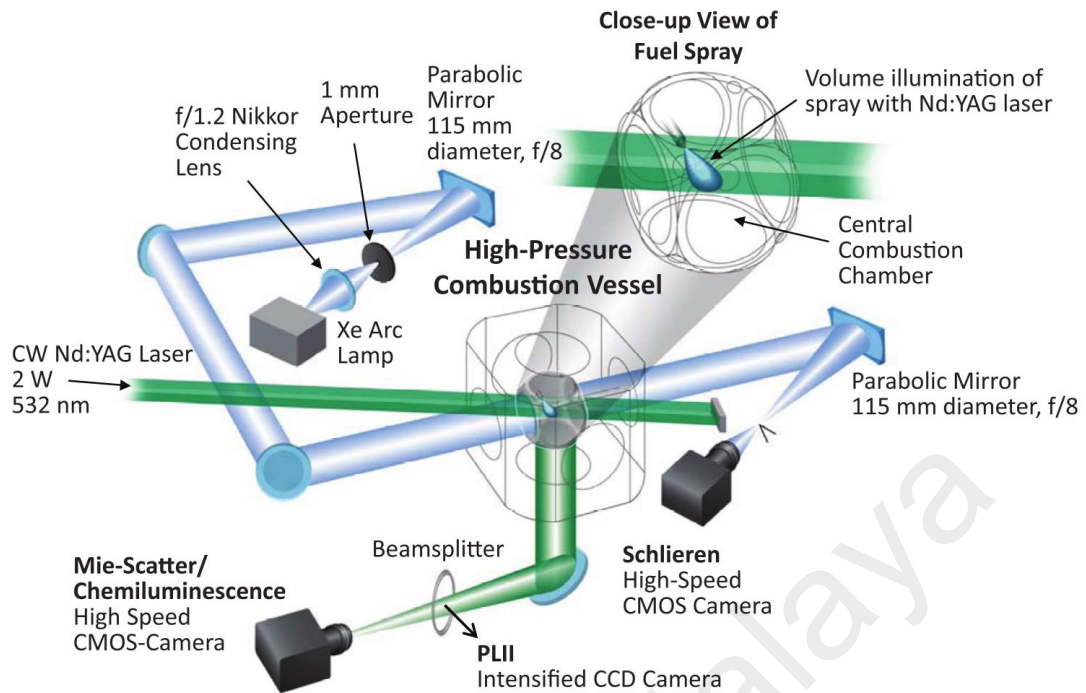


Figure 6.2: Schematic diagram of the optical setup (Nerva et al., 2012).

6.2.2 Numerical Model Configurations

In this study, the spray combustion solver in OpenFOAM-2.0.x is used to perform the constant-volume spray combustion simulations. The reduced kinetic model developed in Chapter 4 is applied here to model the reacting SME fuel spray at operating conditions stated in Table 6.2. It is apparent that the biodiesel feed-stock used in Nerva's experiment is different from the target fuel (i.e. RME) set for the developmental work of the reduced kinetic in Chapter 4. Nonetheless, this may be regarded as acceptable since the difference in the average saturated compositions between these two fuels is relatively small (i.e. ~6%) (Bax et al., 2010; Herbinet et al., 2008) and the experimental data available in the literature is also limited. The actual thermo-physical properties for RME are applied to appropriately simulate the reactive spray development.

Here, an axial-symmetric computational grid is used consistently for all the 2-D spray combustion simulations presented in this Chapter, as illustrated in Figure 6.3.

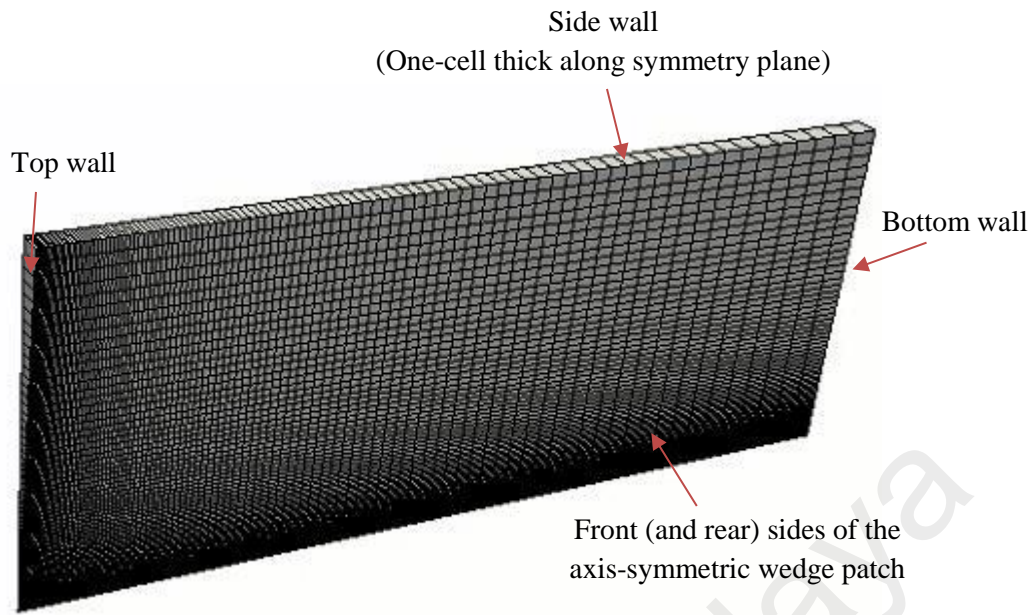


Figure 6.3: Wedge-shaped computational grid for the 2-D spray combustion simulations.

It is evident that the geometry of the wedge mesh is different from that of the cubical-shaped combustion vessel, as illustrated in Figure 6.1. This wedge mesh applied here is essentially a sector mesh, which is developed by defining first a 3-D cylindrical-shaped geometry. Then, both sides (i.e. front and rear sides) of the axial-symmetric domain are specified as wedge patches, with appropriate application of boundary conditions described in Table 6.3. It is worth-mentioning that the angle of this wedge mesh is very small (i.e. $< 5^\circ$), with one-cell thick along the plane of symmetry. Therefore, it can be treated as a 2-D axial-symmetric geometry in this study, which consists of 8,856 cells in total. This computational grid is well-validated through grid independency test in the previous work (Poon et al., 2014). Mesh grading is applied to generate mesh with blocks of hexahedral cells. The minimum grid size is 0.25 mm x 0.25 mm near the injector tip, while the maximum grid size is 4 mm x 2 mm in both radial and axial directions. It is noted that a smaller grid size in axial location is desired in order to obtain accurate predictions of soot location. On the other hand, larger grid size in radial direction further

from injector tip is selected since it does not affect the predictions of the spray penetration profiles. Further descriptions of the numerical models and mesh configurations can be found in the former work.

Table 6.3: Boundary conditions applied in the wedge mesh generation.

Patch(es)	Boundary Condition(s)	Details
Top wall	<i>Wall</i>	No-slip condition and zero pressure gradient
Bottom wall	<i>Wall</i>	
Side wall	<i>Wall</i>	
Front side of axis-symmetric wedge	<i>Wedge</i>	Wedge patch pairs with separation of single-cell layer; Particles snapped to the mid-plane between the wedge patch pairs.
Rear side of axis-symmetric wedge	<i>Wedge</i>	

Furthermore, the CFD sub-models applied in these 2-D spray combustion simulations are listed in Table 6.4. The optimum numerical constants used for each CFD sub-model are validated through parametric studies under non-reacting fuel spray conditions, as detailed in the previous work. Next, the reduced kinetic model is coupled with these CFD sub-models in the subsequent sections to evaluate the model predictions under both non-reacting and reacting spray environments.

Table 6.4: CFD sub-models applied in the 2-D spray combustion simulations.

Spray breakup model	Reitz-Diwakar
Turbulence model	Standard $k-\varepsilon$
Atomization model	Blob Sheet Atomization
Soot model	Multi-Step

6.3 Validation Results Under Non-Reacting Fuel Spray Conditions

In this section, the simulated liquid and vapour penetration lengths under non-reacting environment are compared with those measured from the experiments (Nerva et al., 2012). The results are shown in Figure 6.4. Here, liquid penetration length (LPL) is defined as the axial location from the injector to the location where 99 % of the total liquid mass is obtained. These definitions correspond with those recommended by Engine Combustion Network. On the other hand, vapour penetration length (VPL) is defined as the axial location from the injector in which fuel vapour fraction which is less than 0.001 is found. Based on the results demonstrated in Figure 6.4, it is observed that both LPL and VPL predicted by the reduced biodiesel surrogate fuel model are in good agreement with those of the measurements.

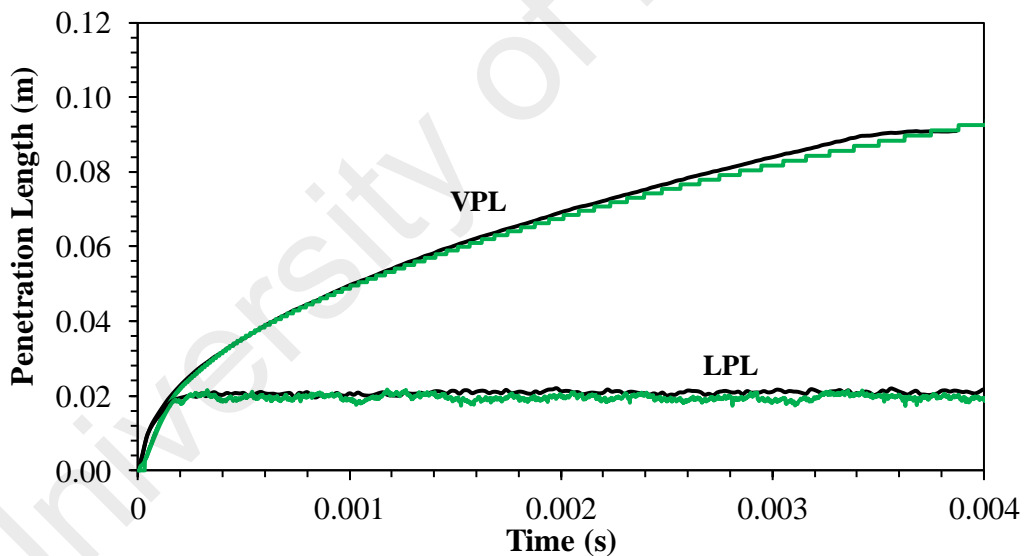


Figure 6.4: Comparisons of the predicted (green) and measured (black) LPL and VPL.

6.4 Validation Results Under Reacting Fuel Spray Conditions

Next, the computed IDs and LOLs by the reduced model are compared with the experiment data of SME fuel oxidations in the constant volume combustion vessel at ambient temperatures of 900 K and 1000 K. The results are presented in Table 6.5. Here,

ID is defined as the maximum dT/dt gradient of the temperature profile, whereas LOL is defined as the distance from the injector to the closest layer in which OH mass fraction reaches 2 % of its maximum value in the domain. These correspond with the definitions published by the Engine Combustion Network.

Table 6.5: Comparisons between the predicted and measured IDs and LOLs at ambient temperatures of 900 K and 1000 K.

Parameter(s)		Measurements	Predictions
ID (μs)	900 K	709	590
	1000 K	377	298
LOL (mm)	900 K	26.18	28
	1000 K	17.27	18

Referring to Table 6.5, overall agreement between the predictions and measurements are achieved for both ambient temperature conditions. However, it is found that the predicted IDs are consistently shorter than the measurements, whereas opposite trends are obtained for LOL predictions. The maximum deviations between the computations and measurements of IDs and LOLs are recorded at 21 % and 7 %, respectively. This can be attributed to the higher amount of unsaturated FAME in RME (i.e. ~94 %) than SME (i.e. ~88 %), which enhances chain branching process as a result of its double bond location at the end of the hydrocarbon chain (Herbinet et al., 2010).

Furthermore, qualitative comparisons of the soot contours predicted by the reduced model with respect to the experimental measurements at quasi-steady state (4ms after start of injection) are performed for ambient temperatures of 900 K and 1000 K. The experimental soot contours are the time-averaged radial SVF distribution plots which are obtained from the combination of qualitative PLII images and the quantitative soot optical thickness measurements at the fuel jet centreline (Nerva et al., 2012). The results are demonstrated in Figure 6.5. It is observed that the qualitative soot distributions simulated

by the reduced model agree reasonably well with the measurements in terms of both soot location and soot length. Besides, highest soot volume fraction is also captured at the centre region of soot clouds. This corresponds with the fuel-rich region of the fuel jet.

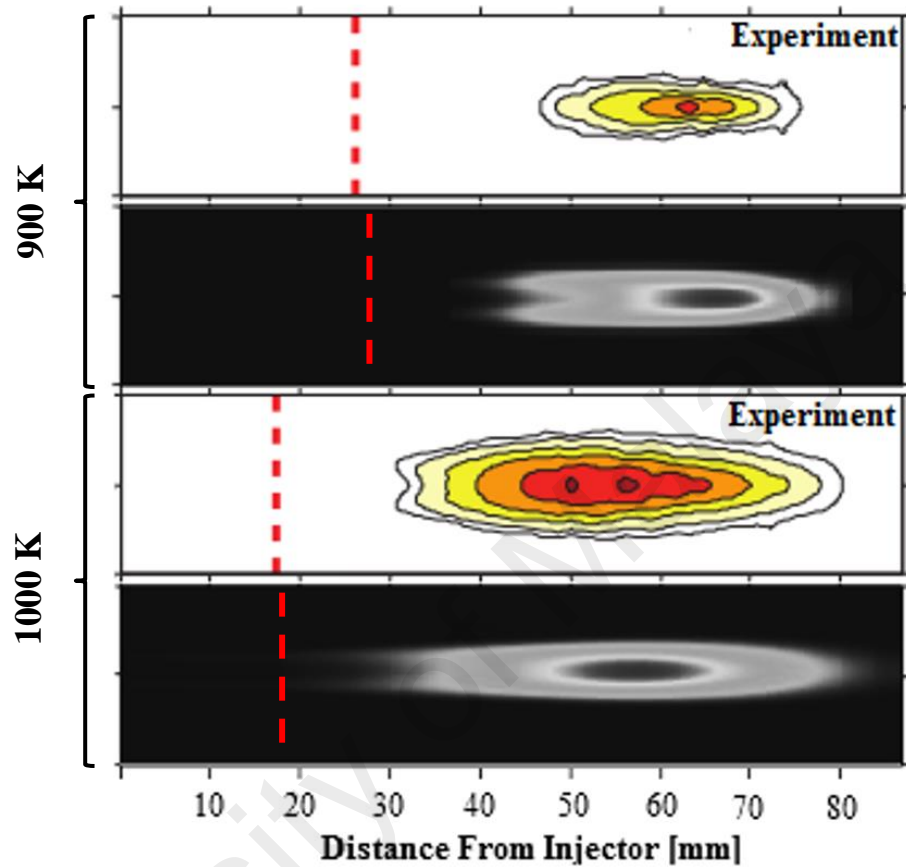


Figure 6.5: Predicted SVF contours and experimental soot cloud images at quasi-steady state for fuel combustions at ambient temperatures of 900 K and 1000 K. Note: Red lines indicate the flame lift-off.

6.5 Chapter Conclusions

In this chapter, the reduced model has been successfully validated with respect to the experimental measurements of SME oxidation in a constant volume vessel through 2-D simulations under both non-reacting and reacting environments. The experimental LPL and VPL are reproduced well, while the computations of IDs and LOLs by the reduced model yield good agreement as compared to the measurements. On the other hand, the experimental soot contours are reasonably replicated in terms of the location and shape of the soot cloud.

CHAPTER 7: VARIATION IN FUEL SATURATION LEVELS

7.1 Introduction

In this chapter, the applicability of the reduced kinetic model as a generic surrogate model for different biodiesel feed-stocks, such as SME, SFME and PME, is examined using the fuel compositions depicted in Section 7.2. Here, validation exercises of the reduced model are first performed in 0-D kinetic simulations under auto-ignition and JSR conditions by using different combinations of saturation/unsaturation composition which matches those of the actual fuels. This is followed by the model validations against the JSR experimental data obtained by Bax et al. (2010) and Hakka et al. (2009). The results are presented in Section 7.3. Subsequently, the surrogate model is applied in 2-D CFD spray combustion simulations to investigate the combustion and soot formation performances of these biodiesel feed-stocks. Simulation results obtained are analysed and discussed in Section 7.4. Lastly, key conclusions are summarised in Section 7.5.

7.2 Surrogate Fuel Compositions

The compositions of the surrogate model are adjusted based on the saturation and unsaturation compositions of the actual fuels, such as SME, SFME and PME, as shown in Table 7.1.

Table 7.1: Compositions of the actual biodiesel fuels and the kinetic model (by mass).

Target fuels	Actual fuel compositions		Model fuel compositions		
	Saturation (%)	Unsaturation (%)	MD (%)	MD9D (%)	n-C ₇ H ₁₆ (%)
SME	~12	~88	6	44	50
SFME	~32	~68	16	34	50
PME	~48	~52	24	26	50

As aforementioned in the previous chapter, MD represents the saturated components of the actual fuel while MD9D represents the unsaturated components. Similar to the RME oxidation experiment carried out by Dagaut et al. (2007) in a JSR under dilution, the composition of n-C₇H₁₆ is set at 50 % by mass. The remaining 50 % of the surrogate fuel compositions is then divided accordingly based on the actual saturated and unsaturated compositions of the fuel.

7.3 Model Validations in 0-D Kinetic Simulations

In this section, the surrogate model is first validated against its detailed counterpart in 0-D kinetic simulations in terms of ID and species concentrations under both auto-ignition and JSR conditions by varying its saturation and unsaturation compositions according to those of the actual fuels provided in Table 7.1. The simulation results are depicted in Section 7.3.1. Next, the fidelity of the surrogate model is further assessed in Section 7.3.2 with respect to the JSR experimental measurements of Bax et al. (2010) and Hakka et al. (2009) using the same combinations of saturation/unsaturation compositions applied in Section 7.3.1.

7.3.1 Validations against Detailed Model under Auto-Ignition and JSR Conditions

The operating conditions illustrated in Table 5.1 are applied. Here, only results for ID predictions at initial pressure of 60 bar and species profiles at initial pressure of 60 bar and Φ of 1 are presented. Same ID pattern is attained for initial pressures of 40 bar and 80 bar.

The ID plots for SME, SFME and PME combustions are shown in Figure 7.1. Reasonably good agreement between the predictions of the reduced and detailed models is achieved for each configuration. Maximum deviation of 43 % is recorded for SME

combustion throughout the tested conditions. This is reasonable as it falls within the acceptable error tolerance range of 30 – 50 % for large-scale mechanism reduction, as demonstrated in some literatures (Brakora et al., 2011; Luo et al., 2012; Niemeyer et al., 2010; Yang et al., 2012).

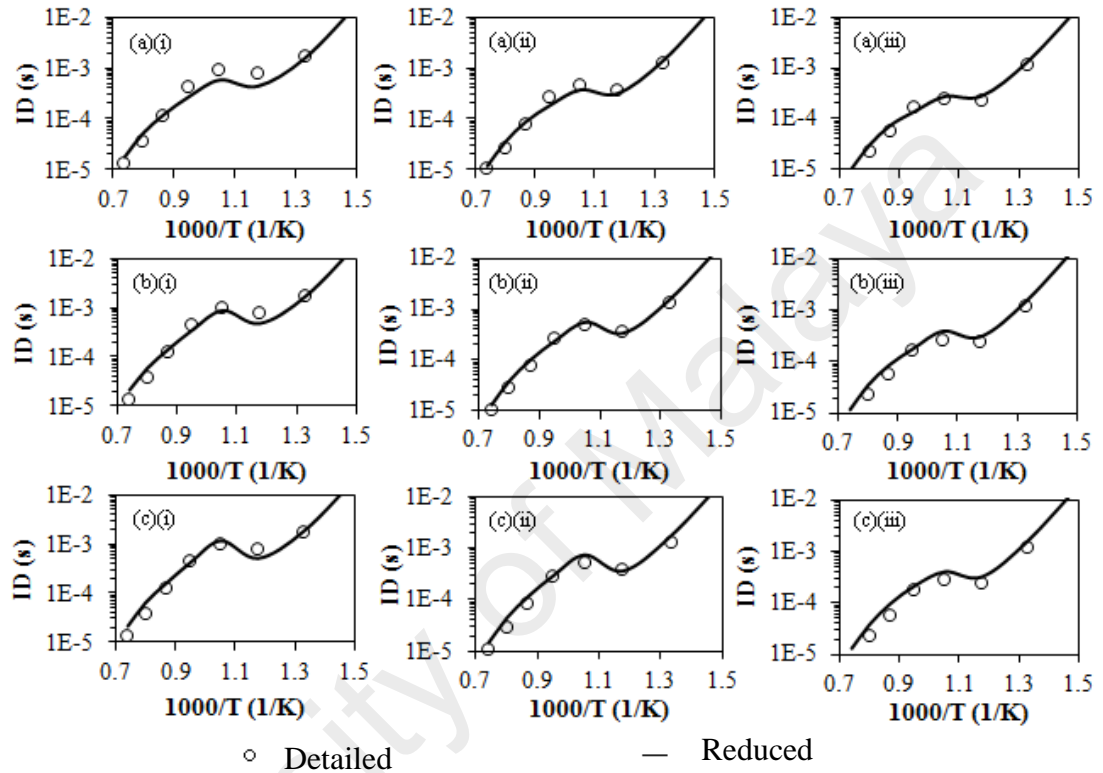


Figure 7.1: Computed ID of (a) SME, (b) SFME and (c) PME calculated by respective detailed and reduced models, with initial pressure of 60 bar and Φ of (i) 0.5, (ii) 1.0, (iii) 2.0.

Nonetheless, it is observed that the deviations between the computations by the reduced and detailed models increase with higher fuel saturation level. The maximum deviation recorded for PME case is approximately 65 %. In spite of these, the predicted trend is expected since the kinetic model is initially developed for RME which contains very low percentage of saturated FAME (i.e. 6 %). On the other hand, PME consists of approximately 48 % of saturated FAME, which is almost eight times greater than that of the RME. For the same reason, greater discrepancies in species profile predictions are

found for PME cases under both auto-ignition and JSR conditions, which can be seen in Figures 7.2 and 7.3, respectively.

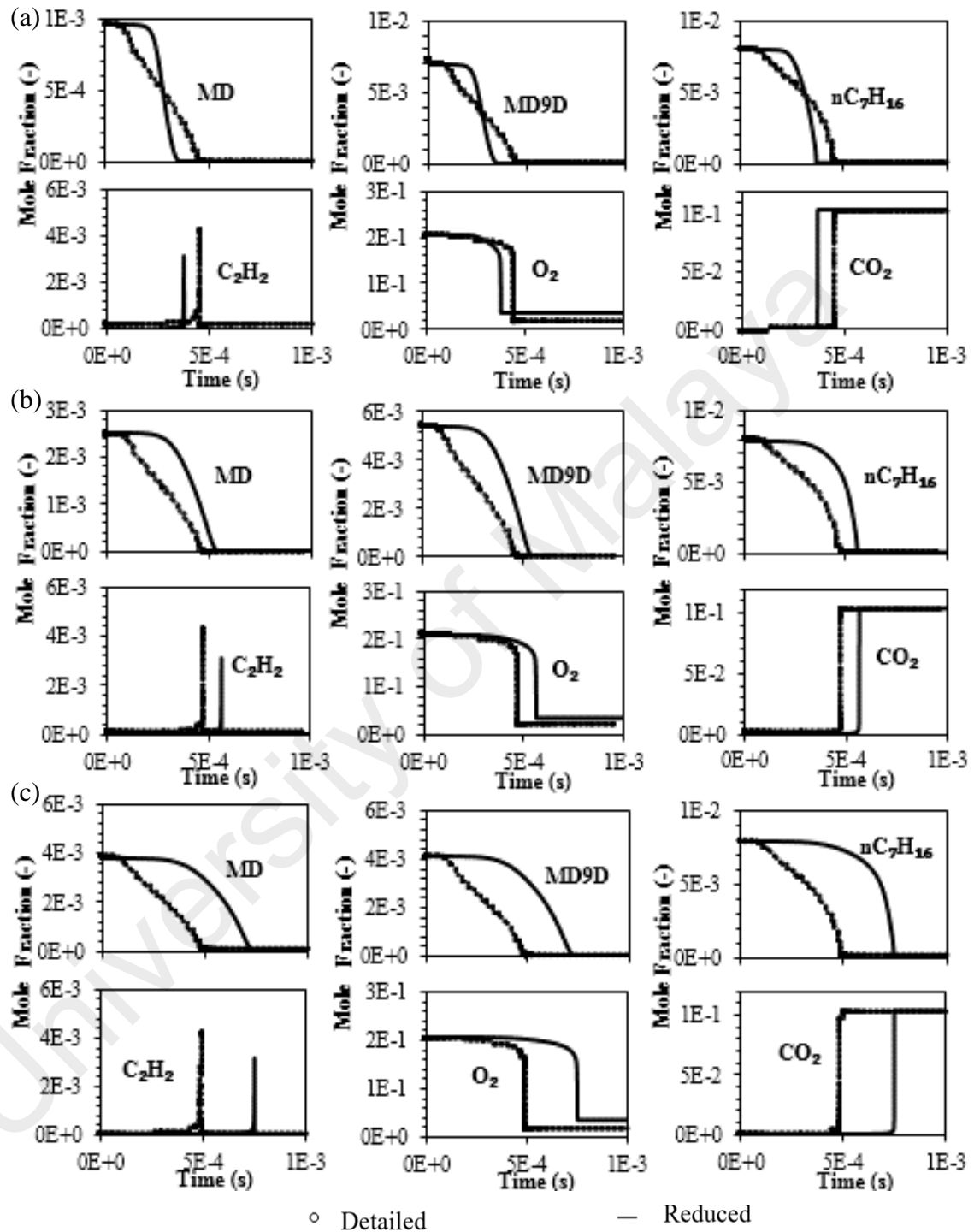


Figure 7.2: Computed species profiles of (a) SME, (b) SFME and (c) PME fuel oxidations under auto-ignition conditions ($P=60$ bar, $\Phi=1.0$, $T=950$ K).

Apart from that, a consistent distance between the calculated species mole fractions using the reduced and detailed models is also observed in Figure 7.2. This corresponds

with the difference in ID predictions between the models, as depicted in Figure 7.1. The current results are considered satisfactory as the reduced model is able to reproduce the temporal evolution trends of the important species fairly well across a wide range of fuel saturation levels. The findings here have demonstrated an acceptable compromise in terms of mechanism size and results accuracy.

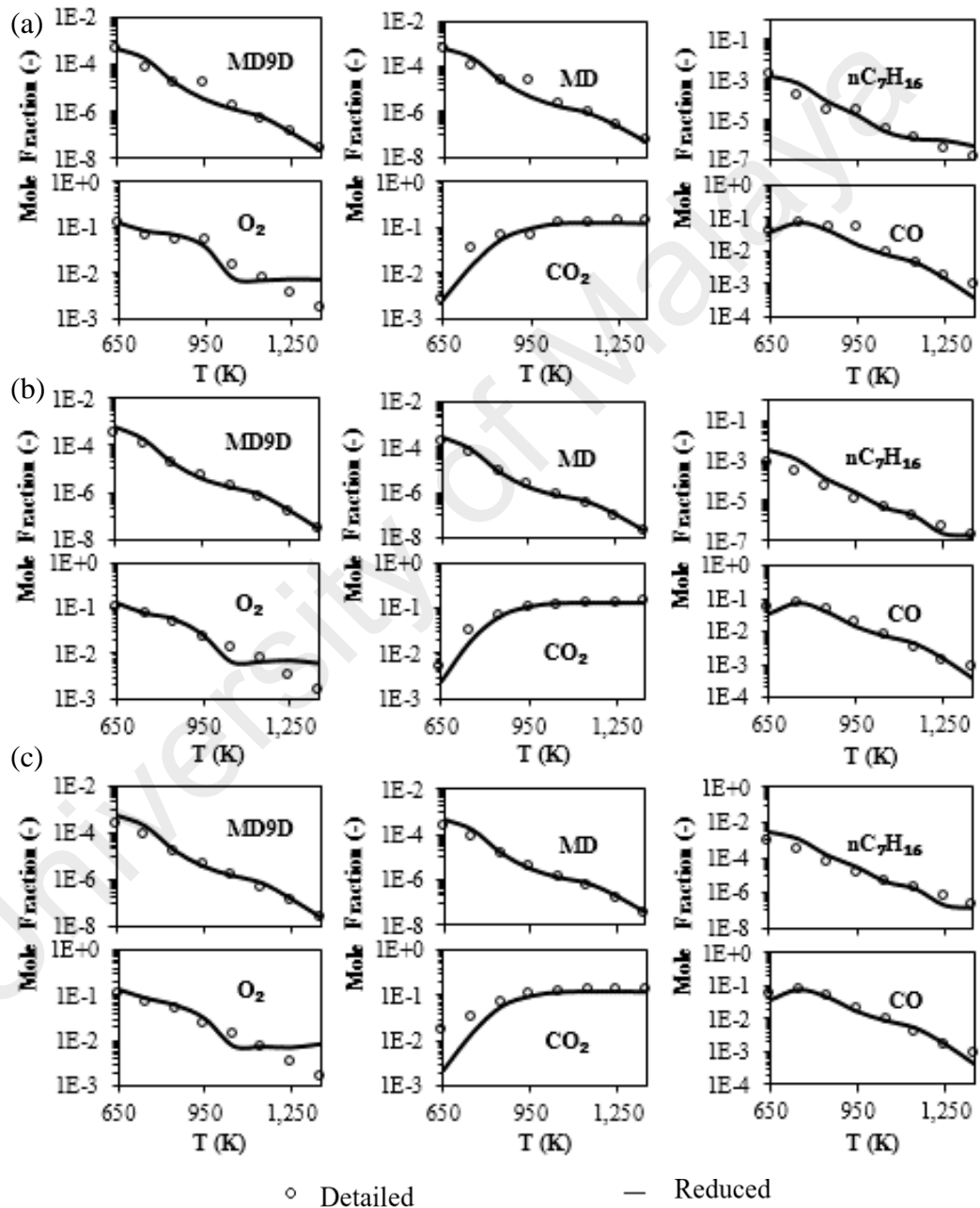


Figure 7.3: Computed species profiles of (a) SME, (b) SFME and (c) PME fuel oxidations under JSR conditions ($P=60$ bar, $\Phi=1.0$, $t_R=0.1$ s).

7.3.2 Validations against JSR Experimental Data

The reduced kinetic model is further validated using the JSR experimental results of methyl oleate/n-decane and methyl palmitate/n-decane oxidations carried out by Bax et al. (2010) and Hakka et al. (2009), respectively. Both methyl oleate and methyl palmitate are selected for benchmark comparisons in this validation work as they are the representative for large unsaturated and saturated FAME, respectively. The compositions of n-decane and methyl oleate/methyl palmitate are set to 26 % and 76 % (in mole), respectively. Same experimental setups are applied for both the biodiesel blends. The fuel-oxygen mixtures are highly diluted by helium and the experiments are performed under stoichiometric condition, at a pressure of 106 kPa, t_R of 1.5 s, and a temperature range of 550 – 1000 K. The inlet fuel mole fraction is 0.002.

The validation results are depicted in Figure 7.4. The experimental measurements for methyl oleate/n-decane and methyl palmitate/n-decane blends are plotted together to draw comparisons between these fuels and the computational results. The selected species for comparison studies here are O_2 , CO_2 , C_2H_2 and C_2H_4 . These species concentrations are validated to ensure that the proposed kinetic model is able to reasonably represent the kinetics of the fuel oxidation. In Figure 7.4, it is observed that the predicted O_2 profiles by the reduced model are identical for all three biodiesel feed-stocks and the computations are also close to the experimental measurements of the methyl oleate/n-decane and methyl palmitate/n-decane blends. The model predictions are also in fairly good agreement with those of the detailed counterpart for all three cases. Besides, it is seen that the overall CO_2 productions computed by both the reduced and detailed models decrease with increment in the fuel saturation level. In contrast, an opposite trend is observed for C_2H_4 and C_2H_6 . These observations are consistent with the measured trends from the experiments (Bax et al., 2010).

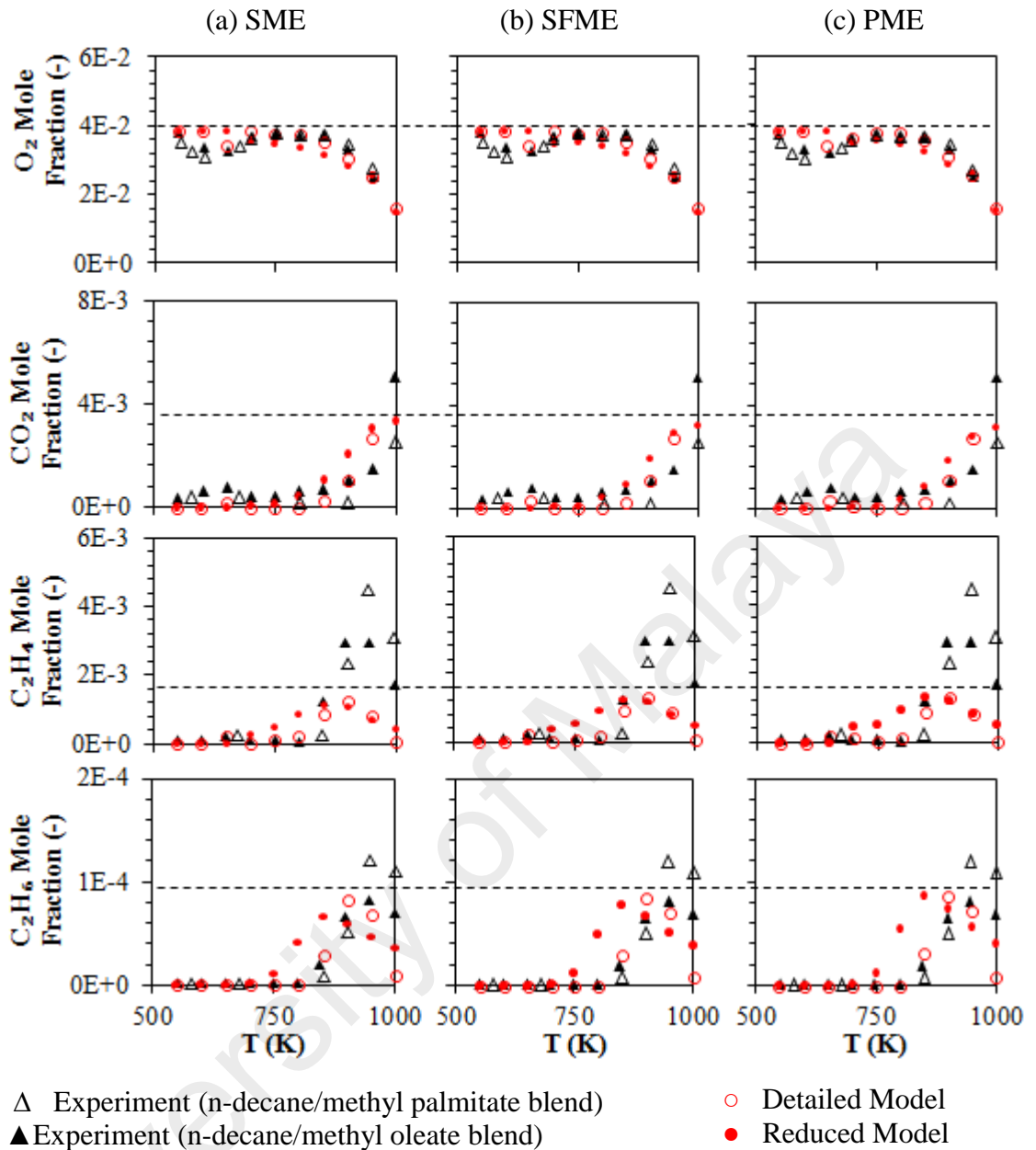


Figure 7.4: Computed and experimental species mole fractions obtained from the oxidation of (a) SME, (b) SFME and (c) PME in a JSR, with initial pressure of 106 kPa, Φ of 1.0 and t_R of 1.5 s. Note: The horizontal dashed lines (--) indicate the maximum species mole fraction predicted by the surrogate models among SME, SFME and PME.

It is noted that the biodiesel fuel blends applied in the simulations consist of a mixture of both saturated and unsaturated esters. On the contrary, the fuel blends used in the experiments only contain either saturated or unsaturated esters. Thus, the computational results might be different from the measurements due to the presence of cross reactions between the saturated and unsaturated FAME. Although variation on the absolute values

of the predicted species mole fractions is apparent as compared to the JSR experimental measurements, the overall agreements in temporal evolution trend between the experimental and computed species profile trends are achieved. The results of the predicted species concentrations are deemed acceptable and the reduced kinetic model is henceforth applied in the next section for further evaluations in the 2-D CFD spray combustion simulations.

7.4 2-D CFD Spray Combustion Simulations

In this section, the combustion characteristics and soot formation performances in response to the variation of fuel saturation level (i.e. SME, SFME and PME) are examined with the use of the reduced kinetic model. The operating conditions and numerical setups employed here are similar to those applied in Chapter 6, which can be found in Table 6.2. Apart from these, the validation results for RME combustion obtained from the earlier 2-D CFD spray combustion simulations are also included for performance benchmarking purposes.

The effects of variation in fuel saturation level on ID and LOL predictions are demonstrated in Figure 7.5. The ambient temperature varies from 900 K to 1000 K while the ambient density is fixed at 22.8 kg/m^3 . In Figure 7.5(a), it is observed that ID becomes longer when the fuel saturation level increases for both ambient temperatures. The predicted IDs are the longest for PME and shortest for RME. As aforementioned, RME contains the highest amount of unsaturated FAME which promotes faster chain branching process and this consequently leads to shorter ID. The findings here agree well with the computational results in the earlier 0-D kinetic simulations in Section 7.3. As a result of shorter ID, the ignition occurs at a location closer to the injection tip and the associated flame lift-off is thus shorter, as demonstrated in Figure 7.5(b).

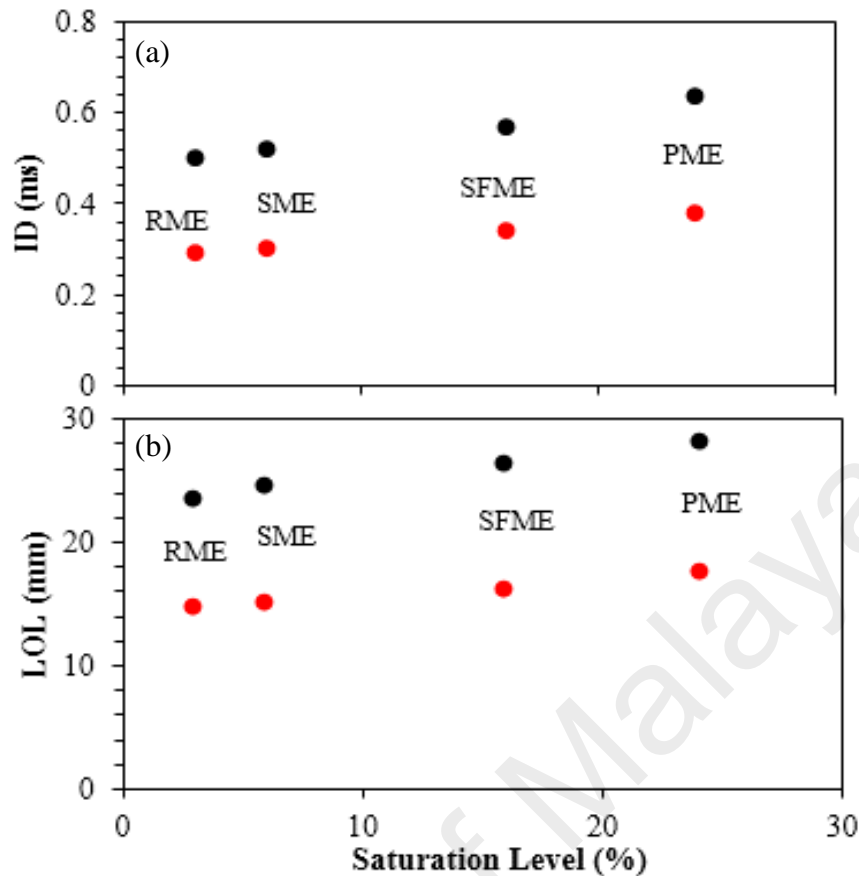


Figure 7.5: Experimental and simulated (a) IDs and (b) LOLs for RME, SME, SFME and PME combustions at ambient temperatures of 900 K (black) and 1000 K (red).

Following that, the SVF predictions of RME, SME, SFME and PME along spray axis at quasi-steady state (i.e. 4 ms after start of injection) for ambient temperatures of 900 K and 1000 K are depicted in Figure 7.6. It is observed that soot is formed at location nearest to the injector tip for RME combustion, followed by SME, SFME and PME for both 900 K and 1000 K cases. This can be attributed to the associated shorter LOLs, as depicted in Figure 7.5(b). In addition, it is found that the predicted SVFs are the highest for RME combustion and lowest for PME combustion for both ambient temperatures. Among all the tested fuels, PME contains the lowest amount of unsaturated fatty acids and hence there are less double bonds in the fuel. It is reported that the presence of double bonds in unsaturated FAME is the key reason for higher production of soot precursors and unsaturated hydrocarbons, which eventually leads to higher engine-out soot emission

(Gail et al., 2008). This trend is well replicated by the model whereby SVF decreases with higher saturation (i.e. lower unsaturation) level.

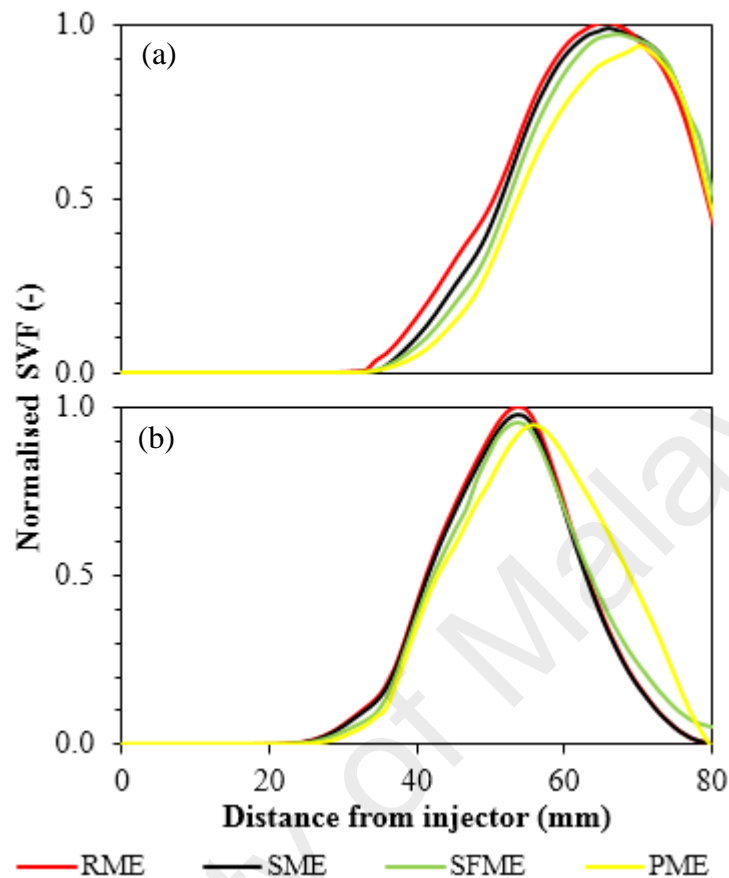


Figure 7.6: Experimental and simulated soot contours at quasi-steady state for RME, SME, SFME and PME combustions at ambient temperatures of (a) 900 K and (b) 1000 K.

7.5 Chapter Conclusions

The compositions of the kinetic model are adjusted according to the saturated and unsaturated levels in different biodiesel feed-stocks, such as SME, SFME and PME. Reasonably well agreement between the reduced and detailed models is obtained for all the different fuel compositions throughout the test conditions in 0-D kinetic simulations. Subsequently, 2-D CFD simulations are carried out using these configurations to compare the combustion and soot formation performances. The predicted IDs and LOLs are found to be lower with greater soot formation when the fuel contains higher unsaturated FAME.

CHAPTER 8: CONCLUSIONS AND FUTURE WORK

8.1 Conclusions

In this work, a reduced kinetic model for RME with only 84 species is successfully derived using a five-stage chemical kinetic mechanism reduction scheme. The model is well-validated in 0-D kinetic simulations under a wide range of auto-ignition and JSR conditions. The overall IDs and species concentration profiles of the detailed model are successfully reproduced by the reduced model with reasonably good agreement and consistency. Apart from these, the temporal evolution trends of the measured species in a JSR are also well captured by the reduced model.

Accordingly, 2-D spray combustion simulations under both non-reacting and reacting environments are performed to further evaluate the fidelity of the reduced model. The simulated and experimental LPL and VPL are in good agreements. On the other hand, satisfactory results are also obtained whereby ID and LOL predictions agree reasonably well with the experiments. The qualitative soot distributions of the experimental soot contours are also reasonably replicated by the reduced model in terms of both soot location and soot length.

In addition, the applicability of reduced model to be used as a generic surrogate model for other biodiesel feed-stocks (SME, SFME and PME) is examined in both 0-D and 2-D simulations by adjusting its saturation/unsaturation compositions. Based on the results obtained in 0-D kinetic simulations, well agreements between the reduced and detailed models are obtained throughout the test conditions for all the composition configurations. Besides, the reduced model is further applied in 2-D simulations to compare the combustion and soot formation performances of various biodiesel feed-stocks using different combinations of saturation/unsaturation compositions. The computed IDs and LOLs are shorter with higher soot productions when the fuel contains higher amount of unsaturated FAME.

The current results suggest that the reduced model serves as a potential surrogate fuel model for biodiesel feed-stocks with low degrees of saturation ($\leq 30\%$), such as the RME, SME and SFME, in both kinetic and CFD spray simulations.

8.2 Suggestions for Future Work

Based on the findings obtained in this study, it is found that the model accuracies in ID and species profile predictions deteriorate rapidly when saturation level is greater than 30 %. Hence, further improvement is necessary such that it can be used as a surrogate model for highly saturated FAME, such as the coconut methyl ester (CME) which contains approximately 80 % of saturated esters in the fuel (Cheng et al., 2015).

University of Malaya

REFERENCES

- An, H., Yang, W. M., Maghbouli, A., Li, J., & Chua, K. J. (2014). A skeletal mechanism for biodiesel blend surrogates combustion. *Energy Conversion and Management*, *81*, 51–59.
- Bax, S., Hakka, M. H., Glaude, P. A., Herbinet, O., & Battin-Leclerc, F. (2010). Experimental study of the oxidation of methyl oleate in a jet-stirred reactor. *Combustion and Flame*, *157*(6), 1220–1229. <https://doi.org/10.1016/j.combustflame.2009.12.008>
- Bongers, H., Van Oijen, J. A., & De Goey, L. P. H. (2002). Intrinsic low-dimensional manifold method extended with diffusion. *Proceedings of the Combustion Institute*, *29*(1), 1371–1378. [https://doi.org/10.1016/S1540-7489\(02\)80168-7](https://doi.org/10.1016/S1540-7489(02)80168-7)
- Bowman, C. T., Hanson, R. K., Davidson, D. F., Gardiner, W. C., Shi, V. L., Smith, G. P., Goldenberg, M. GRI-MECH 2.11. Retrieved from http://www.me.berkeley.edu/gri_mech/
- Brakora, J. L., Ra, Y., & Reitz, R. D. (2011). Combustion Model for Biodiesel-Fueled Engine Simulations using Realistic Chemistry and Physical Properties. *SAE Int. J. Engines*, *4*(1), 931–947. <https://doi.org/10.4271/2011-01-0831>
- Brown, N. J., Li, G., & Koszykowski, M. L. (1997). Mechanism reduction via principal component analysis. *International Journal of Chemical Kinetics*, *29*(6), 393–414. [https://doi.org/10.1002/\(SICI\)1097-4601\(1997\)29:6<393::AID-KIN1>3.0.CO;2-P](https://doi.org/10.1002/(SICI)1097-4601(1997)29:6<393::AID-KIN1>3.0.CO;2-P)
- Cheng, X., Ng, H. K., Gan, S., Ho, J. H., & Pang, K. M. (2015). Development and validation of a generic reduced chemical kinetic mechanism for CFD spray combustion modelling of biodiesel fuels. *Combustion and Flame*, *162*(6), 2354–

2370. <https://doi.org/10.1016/j.combustflame.2015.02.003>

Correa, C., Niemann, H., Schramm, B., & Warnatz, J. (2000). Reaction mechanism reduction for higher hydrocarbons by the ILDM method. *Proceedings of the Combustion Institute*, 28, 1607–1614. [https://doi.org/10.1016/S0082-0784\(00\)80558-5](https://doi.org/10.1016/S0082-0784(00)80558-5)

Curran, H. J., Gaffuri, P., Pitz, W. J., & Westbrook, C. K. (1998). A comprehensive modeling study of n-heptane oxidation. *Combustion and Flame*, 114(1–2), 149–177. [https://doi.org/10.1016/S0010-2180\(97\)00282-4](https://doi.org/10.1016/S0010-2180(97)00282-4)

Curran, H. J., Gaffuri, P., Pitz, W. J., & Westbrook, C. K. (2002). A comprehensive modeling study of iso-octane oxidation. *Combustion and Flame*, 129(3), 253–280. [https://doi.org/10.1016/S0010-2180\(01\)00373-X](https://doi.org/10.1016/S0010-2180(01)00373-X)

Dagaut, P., Gail, S., & Sahasrabudhe, M. (2007). Rapeseed oil methyl ester oxidation over extended ranges of pressure, temperature, and equivalence ratio: Experimental and modeling kinetic study. *Proceedings of the Combustion Institute*, 31(2), 2955–2961. <https://doi.org/10.1016/j.proci.2006.07.142>

Dayma, G., Gail, S., & Dagaut, P. (2008). Experimental and kinetic modeling study of the oxidation of methyl hexanoate. *Energy & Fuels*, (13), 1469–1479. Retrieved from <http://pubs.acs.org/doi/pdf/10.1021/ef700695j>

Diévar, P., Won, S. H., Dooley, S., Dryer, F. L., & Ju, Y. (2012). A kinetic model for methyl decanoate combustion. *Combustion and Flame*, 159(5), 1793–1805. <https://doi.org/10.1016/j.combustflame.2012.01.002>

Engine Combustion Network Experimental Data Archive. Retrieved from <http://www.sandia.gov/ecn/>

- Fisher, E. M., Pitz, W. J., Curran, H. J., & Westbrook, C. K. (2000). Detailed chemical kinetic mechanisms for combustion of oxygenated fuels. *Proceedings of the Combustion Institute*, 28(2), 1579–1586. [https://doi.org/10.1016/S0082-0784\(00\)80555-X](https://doi.org/10.1016/S0082-0784(00)80555-X)
- Gaïl, S., Sarathy, S. M., Thomson, M. J., Diévar, P., & Dagaut, P. (2008). Experimental and chemical kinetic modeling study of small methyl esters oxidation: Methyl (E)-2-butenate and methyl butanoate. *Combustion and Flame*, 155(4), 635–650. <https://doi.org/10.1016/j.combustflame.2008.04.007>
- Gaïl, S., Thomson, M. J., Sarathy, S. M., Syed, S. a., Dagaut, P., Diévar, P., Dryer, F. L. (2007). A wide-ranging kinetic modeling study of methyl butanoate combustion. *Proceedings of the Combustion Institute*, 31(1), 305–311. <https://doi.org/10.1016/j.proci.2006.08.051>
- HadjAli, K., Crochet, M., Vanhove, G., Ribaucour, M., & Minetti, R. (2009). A study of the low temperature autoignition of methyl esters. *Proceedings of the Combustion Institute*, 32(1), 239–246. <https://doi.org/10.1016/j.proci.2008.09.002>
- Hakka, M. H., Glaude, P. A., Herbinet, O., & Battin-Leclerc, F. (2009). Experimental study of the oxidation of large surrogates for diesel and biodiesel fuels. *Combustion and Flame*, 156(11), 2129–2144. <https://doi.org/10.1016/j.combustflame.2009.06.003>
- Herbinet, O., Biet, J., Hakka, M. H., Warth, V., Glaude, P. A., Nicolle, A., & Battin-Leclerc, F. (2011). Modeling study of the low-temperature oxidation of large methyl esters from C₁₁ to C₁₉. *Proceedings of the Combustion Institute. International Symposium on Combustion*, 33(1), 391–398. <https://doi.org/10.1016/j.proci.2010.07.060>

- Herbnet, O., Pitz, W. J., & Westbrook, C. K. (2008). Detailed chemical kinetic oxidation mechanism for a biodiesel surrogate. *Combustion and Flame*, 154(3), 507–528. <https://doi.org/10.1016/j.combustflame.2008.03.003>
- Herbnet, O., Pitz, W. J., & Westbrook, C. K. (2010). Detailed chemical kinetic mechanism for the oxidation of biodiesel fuels blend surrogate. *Combustion and Flame*, 157(5), 893–908. <https://doi.org/10.1016/j.combustflame.2009.10.013>
- Lam, S. H., & Goussis, D. A. (1994). The CSP method for simplifying kinetics. *International Journal of Chemical Kinetics*, 26(4), 461–486. <https://doi.org/10.1002/kin.550260408>
- Le, M. K., & Kook, S. (2015). Injection pressure effects on the flame development in a light-duty optical diesel engine. *SAE International Journal of Engines*, 8(2), 609–624. <https://doi.org/10.4271/2015-01-0791>
- Lee, S. W., & Baik, D. S. (2014). Experimental study on spray and combustion characteristics of biodiesel blends. *International Journal of Bio-Science and Bio-Technology*, 6(2), 91–98. <https://doi.org/10.14257/ijbsbt.2014.6.2.09>
- Leung, K. M., Lindstedt, R. P., & Jones, W. P. (1991). A simplified reaction mechanism for soot formation in nonpremixed flames. *Combustion and Flame*, 87(3–4), 289–305. [https://doi.org/10.1016/0010-2180\(91\)90114-Q](https://doi.org/10.1016/0010-2180(91)90114-Q)
- Li, H., Yang, W., Zhou, D., & Yu, W. (2018). Numerical study of the effects of biodiesel unsaturation on combustion and emission characteristics in diesel engine. *Applied Thermal Engineering*, 137, 310–318.
- Lu, T., Ju, Y., & Law, C. K. (2001). Complex CSP for chemistry reduction and analysis. *Combustion and Flame*, 126(1–2), 1445–1455. <https://doi.org/10.1016/S0010->

- Lu, T., & Law, C. K. (2005). A directed relation graph method for mechanism reduction. *Proceedings of the Combustion Institute*, 30(1), 1333–1341. <https://doi.org/10.1016/j.proci.2004.08.145>
- Lu, T., & Law, C. K. (2006). Linear time reduction of large kinetic mechanisms with directed relation graph: n-Heptane and iso-octane. *Combustion and Flame*, 144(1–2), 24–36. <https://doi.org/10.1016/j.combustflame.2005.02.015>
- Luo, Z., Plomer, M., Lu, T., Som, S., & Longman, D. E. (2011). A reduced mechanism for biodiesel surrogates with low-temperature chemistry. In *7Th US National Combustion Meeting* (pp. 1–10).
- Luo, Z., Plomer, M., Lu, T., Som, S., Longman, D. E., Sarathy, S. M., & Pitz, W. J. (2012). A reduced mechanism for biodiesel surrogates for compression ignition engine applications. *Fuel*, 99, 143–153. <https://doi.org/10.1016/j.fuel.2012.04.028>
- Maas, U., & Pope, S. B. (1992). Simplifying chemical kinetics: Intrinsic low-dimensional manifolds in composition space. *Combustion and Flame*, 88(3–4), 239–264. [https://doi.org/10.1016/0010-2180\(92\)90034-M](https://doi.org/10.1016/0010-2180(92)90034-M)
- Massias, a., & Diamantis, D. (1999). An algorithm for the construction of global reduced mechanisms with CSP data. *Combustion and Flame*, 117(4), 685–708. [https://doi.org/10.1016/S0010-2180\(98\)00132-1](https://doi.org/10.1016/S0010-2180(98)00132-1)
- Meher, L. C., Sagar, D. V., & Naik, S. N. (2006). Technical aspects of biodiesel production by transesterification—a review. *Renewable and Sustainable Energy Reviews*, 10(3), 248–268.

- Metcalf, W. K., Dooley, S., Curran, H. J., Simmie, J. M., El-Nahas, A. M., & Navarro, M. V. (2007). Experimental and modeling study of C₅H₁₀O₂ ethyl and methyl esters. *The Journal of Physical Chemistry. A*, *111*(19), 4001–4014. <https://doi.org/10.1021/jp067582c>
- Mishra, A., & Solanki, H. A. (2016). A Review on biodiesel as efficient alternative fuel energy: Current status and future perspectives. *International Journal of Recent Scientific Research*.
- Mohamed Ismail, H., Ng, H. K., Gan, S., Lucchini, T., & Onorati, A. (2013). Development of a reduced biodiesel combustion kinetics mechanism for CFD modelling of a light-duty diesel engine. *Fuel*, *106*, 388–400. <https://doi.org/10.1016/j.fuel.2012.10.015>
- Nagy, T., & Turanyi, T. (2009). Reduction of very large reaction mechanisms using methods based on simulation error minimization. *Combustion and Flame*, *156*(2), 417–428. <https://doi.org/10.1016/j.combustflame.2008.11.001>
- Nerva, J., Genzale, C. L., Kook, S., Garcia-Oliver, J. M., & Pickett, L. M. (2012). Fundamental spray and combustion measurements of soy methyl-ester biodiesel. *International Journal of Engine Research*. <https://doi.org/10.1177/1468087412456688>
- Niemeyer, K. E., Sung, C. J., & Raju, M. P. (2010). Skeletal mechanism generation for surrogate fuels using directed relation graph with error propagation and sensitivity analysis. *Combustion and Flame*, *157*(9), 1760–1770. <https://doi.org/10.1016/j.combustflame.2009.12.022>
- Pepiot, P., & Pitsch, H. (2005). Systematic reduction of large chemical mechanisms. In

4th Joint Meeting of the U.S. Sections of the Combustion Institute (pp. 1–6).

- Poon, H. M. (2016). *Development of integrated chemical kinetic mechanism reduction scheme for diesel and biodiesel fuel surrogates for multi-dimensional CFD applications*. Graduation Thesis. University of Nottingham.
- Poon, H. M., Ng, H. K., Gan, S., Pang, K. M., & Schramm, J. (2014). Development and Validation of Chemical Kinetic Mechanism Reduction Scheme for Large-Scale Mechanisms. *SAE Int. J. Fuels Lubr.*, 7(3), 653–662. <https://doi.org/10.4271/2014-01-2576>
- Rabitz, H., Kramer, M., & Dacol, D. (1983). Sensitivity analysis in chemical kinetics. *Annual Review of Physical Chemistry*. Retrieved from http://dipartimenti.unicatt.it/dicdr-dipartimenti/dises-sem_090514.pdf
- Ruhul, M. A., Abedin, M. J., Rahman, S. M. A., Masjuki, B. H. H., Alabdulkarem, A., Kalam, M. A., & Shancita, I. (2016). Impact of fatty acid composition and physicochemical properties of Jatropha and Alexandrian laurel biodiesel blends: an analysis of performance and emission characteristics. *Journal of Cleaner Production*, 133, 1181–1189.
- Sankaran, R., Hawkes, E. R., Chen, J. H., Lu, T., & Law, C. K. (2007). Structure of a spatially developing turbulent lean methane–air Bunsen flame. *Proceedings of the Combustion Institute*, 31(1), 1291–1298. <https://doi.org/10.1016/j.proci.2006.08.025>
- Seshadri, K., Lu, T., Herbinet, O., Humer, S., Niemann, U., Pitz, W. J., Law, C. K. (2009). Experimental and kinetic modeling study of extinction and ignition of methyl decanoate in laminar non-premixed flows. *Proceedings of the Combustion Institute*,

32(1), 1067–1074. <https://doi.org/10.1016/j.proci.2008.06.215>

Shi, Y., Ge, H.-W., Brakora, J. L., & Reitz, R. D. (2010). Automatic chemistry mechanism reduction of hydrocarbon fuels for HCCI engines based on DRGEP and PCA methods with error control. *Energy & Fuels*, 24(3), 1646–1654. <https://doi.org/10.1021/ef901469p>

Siebers, D. L. (1998). Liquid-phase fuel penetration in diesel sprays. *SAE Technical Paper Series*, 107(724), 1205–1227. <https://doi.org/10.4271/1999-01-0528>

Sinha, S., Rahman, R. K., & Raj, A. (2017). On the role of resonantly stabilized radicals in polycyclic aromatic hydrocarbon (PAH) formation: pyrene and fluoranthene formation from benzyl–indenyl addition. *Physical Chemistry Chemical Physics*, 19(29), 19262–19278.

Tao, F., Reitz, R. D., & Foster, D. E. (2007). Revisit of Diesel Reference Fuel (n-Heptane) mechanism applied to multidimensional diesel ignition and combustion simulations. In *17th International Multidimensional Engine Modeling User's Group Meeting*, 15, 1–8.

Tomlin, A. S., Turányi, T., & Pilling, M. J. (1997). Mathematical tools for the construction, investigation and reduction of combustion mechanisms. In *Comprehensive Chemical Kinetics* (pp. 293–437).

Turanyi, T. (1990). Reduction of large reaction mechanisms. *New Journal of Chemistry*, 14(11), 795–803.

Turányi, T. (1990). Sensitivity analysis of complex kinetic systems. Tools and applications. *Journal of Mathematical Chemistry*, 5(3), 203–248. <https://doi.org/10.1007/BF01166355>

- Turányi, T., Bérces, T., & Vajda, S. (1989). Reaction rate analysis of complex kinetic systems. *International Journal of Chemical Kinetics*, 21(2), 83–99. <https://doi.org/10.1002/kin.550210203>
- Vajda, S., Valko, P., & Turányi, T. (1985). Principal component analysis of kinetic models. *International Journal of Chemical Kinetics*, 17(1), 55–81. <https://doi.org/10.1002/kin.550170107>
- Valorani, M., Creta, F., Goussis, D., Lee, J., & Najm, H. (2006). An automatic procedure for the simplification of chemical kinetic mechanisms based on CSP. *Combustion and Flame*, 146(1–2), 29–51. <https://doi.org/10.1016/j.combustflame.2006.03.011>
- Valorani, M., & Goussis, D. A. (2001). Explicit time-scale splitting algorithm for stiff problems: auto-ignition of gaseous mixtures behind a steady shock. *Journal of Computational Physics*, 169(1), 44–79. <https://doi.org/10.1006/jcph.2001.6709>
- Van Gerpen, J. (2005). Biodiesel processing and production. *Fuel Processing Technology*, 86(10), 1097–1107.
- Van Oijen, J. A., & De Goey, L. P. H. (2002). Modelling of premixed counterflow flames using the flamelet-generated manifold method. *Combustion Theory and Modelling*, 6(3), 463–478. <https://doi.org/10.1088/1364-7830/6/3/305>
- Vishwanathan, G., & Reitz, R. D. (2009). Modeling soot formation using reduced polycyclic aromatic hydrocarbon chemistry in n-heptane lifted flames with application to low temperature combustion. *Journal of Engineering for Gas Turbines and Power*. <https://doi.org/10.1115/1.3043806>
- Westbrook, C., Naik, C., Herbinet, O., Pitz, W. J., Mehl, M., Sarathy, S. M., & Curran, H. J. (2011). Detailed chemical kinetic reaction mechanisms for soy and rapeseed

biodiesel fuels. *Combustion and Flame*, 158(4), 742–755. Retrieved from <http://www.sciencedirect.com/science/article/pii/S001021801000310X>

Wold, S., Esbensen, K., & Geladi, P. (1987). Principal component analysis. *Chemometrics and Intelligent Laboratory Systems*, 2(1–3), 37–52. [https://doi.org/10.1016/0169-7439\(87\)80084-9](https://doi.org/10.1016/0169-7439(87)80084-9)

Yang, J., Johansson, M., Naik, C., Puduppakkam, K., Golovitchev, V., & Meeks, E. (2012). 3D CFD modeling of a biodiesel-fueled diesel engine based on a detailed chemical mechanism. *SAE Technical Paper*. <https://doi.org/10.4271/2012-01-0151>

Zagaris, A., Kaper, H. G., & Kaper, T. J. (2004). Analysis of the Computational Singular Perturbation reduction method for chemical kinetics. *Journal of Nonlinear Science*, 14(1), 59–91. <https://doi.org/10.1007/s00332-003-0582-9>

Zhang, S., Broadbelt, L. J., Androulakis, I. P., & Ierapetritou, M. G. (2012). Comparison of biodiesel performance based on HCCI engine simulation using detailed mechanism with on-the-fly reduction. *Energy & Fuels*, 26(2), 976–983.

Zhang, Y., Yang, Y., & Boehman, A. L. (2009). Premixed ignition behavior of C₉ fatty acid esters: A motored engine study. *Combustion and Flame*, 156(6), 1202–1213.

Zheng, X. L., Lu, T. F., & Law, C. K. (2007). Experimental counterflow ignition temperatures and reaction mechanisms of 1,3-butadiene. *Proceedings of the Combustion Institute*, 31(1), 367–375. <https://doi.org/10.1016/j.proci.2006.07.182>

Zhu, L., Cheung, C. S., & Huang, Z. (2016). Impact of chemical structure of individual fatty acid esters on combustion and emission characteristics of diesel engine. *Energy*, 107, 305–320.

LIST OF PUBLICATIONS AND PAPERS PRESENTED

1. Poon, H.M., Ng, H. K., Gan, S. and Chong, W. T. (2018). Development of a Reduced Biodiesel Surrogate Fuel Model for Multi-Dimensional CFD Simulations. Paper presented at the International Conference on Sustainable Engineering and Green Technology, Kuala Lumpur, Malaysia. (Accepted for publication)

University of Malaya